

**MINISTRY OF EDUCATION
AND TRAINING**

**VIET NAM ACADEMY OF
SCIENCE AND TECHNOLOGY**

GRADUATE UNIVERSITY OF SCIENCE AND TECHNOLOGY

.....****.....

LE THI TUYET NGAN

**CORRELATION BETWEEN GRIFFITH PHASE AND
MAGNETIC, MAGNETOCALORIC PROPERTIES
OF $\text{La}_{1-x}(\text{Ca,Sr})_x\text{Mn}_{1-y}(\text{Cu,Co})_y\text{O}_3$ SYSTEM**

Specialized: Electronic materials

Numerical code: 9.44.01.23

SUMMARY OF DOCTORAL IN MATERIALS SCIENCE

Ha Noi, 2023

The thesis was accomplished in: Graduate University of Science and Technology - Vietnam Academy of Science and Technology.

Science supervisor:

- 1. Assoc. Prof. Pham Thanh Phong**
- 2. Assoc. Prof. Nguyen Van Dang**

Reviewer 1:.....

Reviewer 2:.....

Reviewer 3:.....

The thesis will be defended in front of the Institute of Doctoral Dissertation Assessment Council, taking place at the Graduate University of Science and Technology - Vietnam Academy of Science and Technology at,, 2023,

People can find this thesis at:

- National library
- Graduate university of Science and Technology library

INTRODUCTION

The lanthanide manganites $\text{Ln}_{1-x}\text{A}'_x\text{MnO}_3$ (Ln is a rare earth element, A' is a divalent, monovalent metal, or vacancy) have attracted considerable attention due to their remarkable physical properties such as Colossal Magneto-resistance effect (CMR), large magnetocaloric effect (MCE),... Recently, several studies of the occurrence of the Griffith phase (GP) and its correlation with the magnetic and magnetocaloric properties of manganite materials that have expanded research topics on these materials, thereby that make the understanding of their physical properties. First theories such as double exchange interaction (DE), Jahn-Teller distortion, and phase separation were proposed to explain the physical nature of manganites. However, the occurrence of magnetic multiphase phenomena and the diverse conductivity of manganites require the addition of several new models to be able to explain more accurately the physical properties of manganites, typically the relationship between critical behavior and magnetic properties, as well as the occurrence of irregularities in the paramagnetic region of doped manganites.

Within in the terms of critical behavior of manganites at Curie temperature (T_C), so far, many studies have shown that manganites almost do not strictly obey any theoretical model. Empirical values of critical exponents often deviate from theoretical models. Even in the same compound, many different results were reported for these values. There are many reasons to explain the aforementioned difference, and naturally, the question of whether the Griffith phase is one of the causes affecting the critical behavior of mangnaties is also set to be studied.

Therefore, the study of anomalies and effects of the appearance of polarons as well as the Griffith phase on electromagnetic properties is a new topic in solid-state physics. Originally, the Griffith phase was understood to be the magnetic phase that exists in Ising's ferromagnetic systems, in which part of the magnetic bond disappears with the appearance of ferromagnetic clusters in the paramagnetic phase of the material. Theoretically, the Griffith phase only occurs in Ising's dilution systems, but later research has shown that this phase can also occur in other ferromagnetic systems (such as the Heizenberg model, etc.), and its identification has been extended through various experimental techniques. The most noticeable sign of the Griffith phase is identified by the downturn of the inverse susceptibility versus the temperature plot from the Curie-Weiss law in the paramagnetic phase. However, this sign is common to both the Griffith phase and ferromagnetic polarons in the paramagnetic region. Without paying attention to standards and other empirical evidence, the conclusions made about the multi-magnetic phases of materials will not be convincing. Therefore, the study of the conditions of Griffith phase occurrence and its influence on physical properties, especially critical parameters, magnetocaloric effects, and electrical conductivity properties of manganites, is one of the important contents that need to be clarified.

Among the lanthanide manganites, $\text{La}_{1-x}\text{Ca}_x\text{MnO}_3$ (LCMO) and $\text{La}_{1-x}\text{Sr}_x\text{MnO}_3$ (LSMO) are the two families that characterize the most important properties of manganites. In particular, the doping of metal ions in the position of La(Ca, Sr) or Mn makes the structure, magnetic properties, electrical conductivity, MCE, CMR effects change very quickly. $\text{La}_{0.7}\text{Ca}_{0.3}\text{MnO}_3$ and $\text{La}_{0.7}\text{Sr}_{0.3}\text{MnO}_3$ compounds are the two materials most often studied because they are typical ferromagnetic manganites. If $\text{La}_{0.7}\text{Ca}_{0.3}\text{MnO}_3$ is a material with a large magnetic entropy change (ΔS_M) but is a first order magnetic phase transition, it is often subject to thermal delay when magnetized, so in refrigeration applications, this will affect the quality of the equipment. While $\text{La}_{0.7}\text{Sr}_{0.3}\text{MnO}_3$ belongs to the second order magnetic phase transition, although the magnetic entropy change (ΔS_M) is a smaller one, due to the absence of thermal hysteresis and a wide working temperature range, it is clearly better to be economical when applied in refrigeration

techniques. From the above analysis, the search for materials with full advantages of the above two materials is the effort of many research groups over the world. Accordingly, the seeking materials which have enough advantages of both materials afore mentioned are the effort of studying groups on the world. Studies of this topic indicate that by changing the fraction ratios of La and Ca/Sr to an appropriate ratio or it is possible to partially replace La, Ca/Sr and Mn by other metal ions; or changing the particle size of the above materials not only partially satisfies the criteria of applications in refrigeration techniques at room temperature but also supports to further understand the physical properties of manganites. Moreover, the changing material's fabrication parameters will also give rise to new magnetic phases, including the Griffith phase, which will make the physical picture in the material more complex, however in-depth study of it will provide interesting information about the role of magnetic phases in the correlations between magnetic properties, conductive properties and other important effects of the material.

Guo and colleagues found the maximum magnetic entropy change value of 300nm - $\text{La}_{0.75}\text{Ca}_{0.25}\text{MnO}_3$ at $T_C = 224$ K under a 1.5 T magnetic field to be about 4.7 J/kgK. This value is greater than the value of Gd under the same conditions of the external magnetic field (4.2 J/kgK at $T_C = 293$ K). Therefore, continuing to study in depth the magnetic properties of this material as well as manganites with a Ca concentration around 0,25 is an important and interesting topic. For this reason, we selected and fabricated the nano $\text{La}_{1-x}\text{Ca}_x\text{MnO}_3$ ($x = 0.20, 0.22, \text{ and } 0.25$) system by sol-gel method to study and find the interesting physical characterizations of this system.

In addition to changing the particle size, many studies have also shown that dosing metal ions into the Mn site is also an effective and feasible solution that not only enhances the value of ΔS_M at room temperature, but also changes the magnetic structure and conductivity of the material, promising to observe many interesting physical effects. Among commonly used metal ions, the nonmagnetic - Cu and the magnetic - Co ions are two metal ions that exhibit many complex properties when doped into site of Mn ions.

Theoretical studies combined with experiments show that Cu ions in $\text{La}_{0.7}\text{Sr}_{0.3}\text{Mn}_{1-x}\text{Co}_x\text{O}_3$ materials can exist in all three different valences, that is +1, +2, and +3. This greatly affects the structure and physical properties of this material system. Studies on the influence of Cu on the magnetic properties of the system show that the T_C of the system is almost constant until the concentration of Cu is not more than 0,04 ($x \leq 0,04$) and the value of Cu is also quite large compared to other manganite materials. However, there has not been any works to investigate the effect of higher Cu concentrations on the structure and other physical properties of the material, so the choice of doping the concentration of Cu is higher than a new problem set out to continue the research. Among the magnetic ions, the Co ion exhibits many valence characteristics and complex spin state. It can exist in valence +2, +3, and +4 and the spin state can be low spin, intermediate spin and high spin. Therefore, doping the Co ions into the site of Mn will arise many physical characteristics related to both its valence and its spin state. So far, most of the research on this issue has only focused on two main systems, namely $\text{La}_{1-x}\text{Sr}_x\text{CoO}_3$ and $\text{La}_{1-x}\text{Ca}_x\text{CoO}_3$. The results obtained are very different, especially the spin state of Co in the material. Depending on the spin state of Co, their magnetic properties come from antiferromagnetism to ferromagnetism to glass spin, or they may simultaneously exist in all three magnetic phases in the same material. The diversity and complexity of magnetic properties in the $\text{La}_{1-x}\text{Sr}_x\text{CoO}_3$ and $\text{La}_{1-x}\text{Ca}_x\text{CoO}_3$ systems have made them interesting and that continue to be of interest to the solid-state physics community in recent years, despite decades of intensive research related to these two systems. However, the spin state of the Co ion as well as the role of the Griffith phase (if any) on the physical properties of the $\text{La}_{0.7}\text{Sr}_{0.3}\text{Mn}_{1-x}\text{Co}_x\text{O}_3$ system

have so far not been deeply studied, so the choice of doping Co ions into the Mn position with different concentrations to investigate their influence on the electrical-magnetic properties of the $\text{La}_{0.7}\text{Sr}_{0.3}\text{Mn}_{1-x}\text{Co}_x\text{O}_3$ system is also a problem that continues to be solved.

The selection of the above three material systems for fabrication and research is not only to understand the above problems but, more importantly, whether the Griffith phase appears in those materials and Griffith phase effects on other physical properties of the material. This is the main research content of the dissertation. Manganites are not only a very interesting research topic but also a potential material for application in many different fields of engineering and life. Based on the actual situation and research conditions, such as experimental equipment, references, and the possibility of research collaboration with domestic and foreign research groups, we consider that the research and solving of the above-mentioned problems is completely feasible and can give many positive results. For these reasons, we have chosen the research problem of the dissertation: ***“Correlation between Griffith phase and magnetic, magnetocaloric properties of $\text{La}_{1-x}(\text{Ca},\text{Sr})_x\text{Mn}_{1-y}(\text{Cu},\text{Co})_y\text{O}_3$ system.”***

The target of the dissertation

The objectives of the thesis are: (i) to find the cause of Griffith phase occurrence (if any) and elucidate the effect of Griffith phase occurrence (if any) on the magnetocaloric effect, the critical parameters in nano $\text{La}_{1-x}\text{Ca}_x\text{MnO}_3$ ($x = 0.20, 0.22, 0.25$) materials and bulk $\text{La}_{0.7}\text{Sr}_{0.3}\text{Mn}_{1-x}\text{M}_x\text{O}_3$ ($\text{M} = \text{Cu}$ and Co) materials; (ii) to determine the effect of particle size and the doping of non-magnetic ions (Cu) and magnetic ions (Co) on the magnetic properties of the three material systems; and (iii) from experimental data, to study and evaluate the correlation between the magnetocaloric effect, the critical parameters of the above materials under the conditions of magnetic multiphase.

The main theme of the dissertation

Simultaneously with the experimental data obtained, we analyzed and argued the effect of Griffith phase on magnetocaloric effects, critical parameters, and the relationship between these properties in the material. The content of the dissertation includes an overview of the perovskite material ABO_3 (structure, magnetic properties, and conductivity of the material), experimental techniques, research results on the effect of particle size on the physical properties of the nanomaterial $\text{La}_{1-x}\text{Ca}_x\text{MnO}_3$ system ($x = 0.20, 0.22,$ and 0.25) and the effect of non-magnetic ions (Cu) and magnetic ions (Co) on the physical properties of the $\text{La}_{0.7}\text{Sr}_{0.3}\text{Mn}_{1-x}\text{M}_x\text{O}_3$ ($\text{M} = \text{Cu}$ and Co) system.

This dissertation includes five chapters:

Chapter 1. Structure and magnetism of manganite materials

Chapter 2. Magnetocaloric effects and critical exponents in manganites

Chapter 3. Experimental Techniques

Chapter 4. Study of magnetic properties, magnetocaloric effects, and critical exponents in the nano $\text{La}_{1-x}\text{Ca}_x\text{MnO}_3$ ($x = 0.20, 0.22,$ and 0.25) system.

Chapter 5. Effect of doped-Cu ions on magnetic properties, critical behavior, magnetocaloric, and Griffith phase in the $\text{La}_{0.7}\text{Sr}_{0.3}\text{Mn}_{1-x}\text{Cu}_x\text{O}_3$ system and the effect of doped-Co ion on magnetic properties and Griffith phase in the $\text{La}_{0.7}\text{Sr}_{0.3}\text{Mn}_{1-x}\text{Co}_x\text{O}_3$ system.

The main results of the dissertation have been published in 08 articles, including 07 ISI articles and one national article.

CHAPTER 1. STRUCTURE AND MAGNETIC PROPERTIES OF MANGANITES MATERIALS

1.1. Crystal structure, magnetic structure, and magnetic phases of manganites

The phase diagrams of the $\text{La}_{1-x}\text{Sr}_x\text{MnO}_3$ system and the $\text{La}_{1-x}\text{Ca}_x\text{MnO}_3$ system demonstrate that anomalous variations of the magnetic state are observed, particularly in the upper proximity of the T_C temperature, leading to the formation of the magnetic multiphase state. On the paramagnetic backdrop, there are also a few ferromagnetic clusters that are confined. In doped manganites, the struggle between magnetic interactions has resulted in a variety of intriguing states and phenomena, including the Griffith phase, dielectric metal phase transitions (M-I), and charge-ordered phase transitions (CO). What is this Griffith phase? We describe the nomenclature and primary physical attributes of this new magnetic phase in the next section.

1.2. Griffith phase appearance in manganites

1.2.1. Griffith phase and Griffith model

Griffiths (1969) first described, in a randomly diluted Ising ferromagnetic system in which only part of the lattice cell sites are occupied by spins. This anomalous property exists in the temperature range $T_C^{rand} < T < T_G$, where T_C^{rand} is the disorder dependent FM ordering temperature and T_G is the Griffith temperature. Due to the dispersion of the ferromagnetic spin clusters in the paramagnetic phase, the short-range ferromagnetic order localizes in the sample and forms a new magnetic phase called the ‘‘Griffith phase’’ (GP).

According to the Griffith model, the Griffith phase only appears in spin systems that are consistent with the random Ising model. However, rather than adhering to the Ising model, the majority of the aforementioned alloys and complex oxides, including doped manganites, follow the Heisenberg three-dimensional (3D) random pattern. As a result, to identify the GP phase in manganites, additional physical models with unique standards must be used in addition to the original GP model (the Ising model of word dilution and the random Ising model).

1.2.2. Signs and methods of determining Griffith phase

Initially, the Griffith phase was thought to be the magnetic state that exists in an ising ferromagnet system that has been randomly diluted, during which a portion of the magnetic bond vanishes and ferromagnetic clusters start to form in the material's paramagnetic phase. Ising ferromagnet systems with randomly diluted Griffith phases can also be found in nanosystems.

Figure 1.9 shows that one of the important characteristics of GP is the deviation from Curie -Weiss's law of paramagnetic induction in a low magnetic field at a temperature $T \approx T_G > T_C$. The change in the slope of the curve $\chi^{-1}(T)$ well above T_C allows for a possible Griffiths singularity. In the region $T_C(p) < T < T_G$, the system is characterized by the coexistence of FM clusters within the globally paramagnetic (PM) phase, which is referred to as the GP or magnetic polaron.

In those manganites, the GP is usually characterized by several features that occur

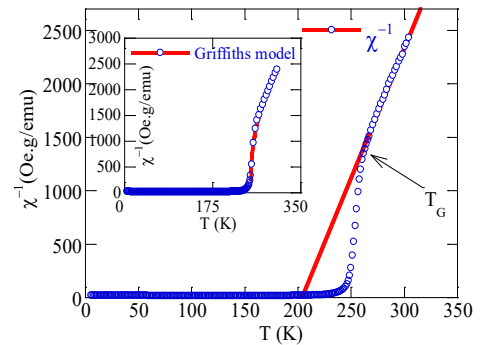


Fig. 1.9. Variation of the inverse of the susceptibility ($1/\chi$) with temperature for sample $\text{La}_{0.7}\text{Ca}_{0.3}\text{MnO}_3$. The straight, solid line indicates the best fit of the Curie-Weiss law in the paramagnetic range ($T > T_G$). The solid lines in the inset are the fit with the power law equation (1.4).

simultaneously: (i) As the temperature drops to T_C , the inverse susceptibility $\chi^{-1}(T)$ in low magnetic fields deviates sharply from the high-T Curie-Weiss (CW) behavior because the FM cluster contribution enhances the low-field magnetization. (ii) Due to the polarization of spins outside of the clusters, the deviation is suppressed in large magnetic fields. The inverse magnetic susceptibility $\chi^{-1}(T)$ follows the Curie-Weiss function: $\chi^{-1}(T) = C/(T - \theta_{CW})$ (1.3) in which C is the Curie constant, and θ_{CW} is the Curie-Weiss temperature. (iii) The low-field susceptibility in the GP region obeys the power law: $\chi^{-1}(T) \sim (T - T_C^{Rand})^{1-\lambda_{GP}}$ ($0 < \lambda_{GP} < 1$ with $0 < \lambda < 1$) (1.4) where C is the Curie constant and θ_p is the Weiss temperature. The polarization of the spins on the ferromagnetic clusters' surface is assumed to be the cause. (iv) A much larger the experimental effective paramagnetic moment than the theoretical effective paramagnetic moment that due to the contribution of FM clusters containing more than two Mn ions.

The following steps can be used to summarize the procedure for determining the GP phase:

Step 1: Conduct a detailed survey of the variation of the inverse of the susceptibility (defined as $\chi^{-1} = H/M$) with temperature in various magnetic fields.

Step 2: Fit the variation of the inverse of the susceptibility ($1/\chi$) with temperature lines according to Equations (1.3) and (1.4), combined with the following GP occurrence conditions:

+ GP only appears in the magnetic disorder temperature range and Griffiths temperature $T_C^{Rand} < T < T_G$ region, where $\chi^{-1}(T)$ deviates from the Curie-Weiss behavior below which the FM clusters emerge in the PM matrix, as is described in a Griffiths phase system. Determine the temperature T_G and T_C^{Rand} . The temperature T_G determines the upper limit for the existence of the Griffiths phase and is simultaneously the temperature of the transition into the paramagnetic phase and disordered temperature T_C^{Rand} , the temperature at which an infinite ferromagnetic cluster forms, depends on the degree of disorder in the system and determines the lower limit for the existence of the Griffiths phase.

+ In the paramagnetic area, the low-field susceptibility in the GP should obey the following power law: $\chi^{-1}(T) \sim (T - T_C^{Rand})^{1-\lambda_{GP}}$ ($0 < \lambda_{GP} < 1$) (1.4); in large magnetic fields, the inverse susceptibility $\chi^{-1}(T)$ obeys the Curie - Weiss law. Griffiths coefficient λ_{GP} satisfies the condition ($0 < \lambda_{GP} < 1$), temperature T_C^{Rand} and temperature T_G are determined by fitting the data $\chi^{-1}(T)$ according to Equation (1.4). Besides, to estimate λ_{PM} , λ_{GP} accurately and T_C^{Rand} , we have followed the method by A.K. Pramanik and A. Banerjee.

Step 3: Compare the value of effective spin and an effective Mn ion (the weighted average of $S_{Mn^{4+}}=3/2$ and $S_{Mn^{3+}}=2$) or the experimental effective paramagnetic moment and the theoretical effective paramagnetic moment. According to the characteristics of GP, much larger effective spin or the experimental effective paramagnetic moment proves the presence of GP.

On the other hand, another important sign to identify the GP phase is the short-range FM ordering, so there will be no spontaneous magnetization in the $T_C < T < T_G$ region. This is one of the additional important criteria to help identify GP more accurately.

1.3.2. Griffith phase diagram in some manganites systems

By comparing the studies of the authors (Vietnam and the world) and analyzing the conditions of GP occurrence in the phase diagram of three typical manganite systems: $La_{1-x}Sr_xMnO_3$, $La_{1-x}Ca_xMnO_3$, $La_{1-x}Ba_xMnO_3$, we find that it is clear that GP only appears at certain doping concentrations and does not follow the Ising model. GP studies later also show that the cause of the current GP is controversial; even some reports suggest that the Griffith phase may occur in manganese nanomaterials.

Obviously, studies of GP on individual manganites have undoubtedly been extensively conducted, but it is difficult to provide a generalized picture of GP occurrence and its explanation in bulk material

systems doped with manganite nanomaterials and other metal ions. Furthermore, the creation of the Griffith phase and its impact on the electrical and magnetic characteristics of doped manganite systems have not received much attention in domestic investigations. As a result, we continue to research whether GP occurs in the $\text{La}_{1-x}\text{Ca}_x\text{MnO}_3$ ($x = 0.20, 0.22$ and 0.25) nanosystem and the $\text{La}_{0.7}\text{Sr}_{0.3}\text{MnO}_3$ system of Cu and Co ion doping on the position of Mn as well as its potential impact (if any) on the material's physical properties. The research results are detailed and specific in Chapters 4 and 5 of the thesis.

CHAPTER 2. THE MAGNETOCALORIC EFFECT AND THE CRITICAL EXPONENTS IN MANGANITE MATERIALS

In this chapter, we present the relationship between the magnetocaloric effect and the critical exponents in manganite materials with GP appearance to illustrate the various viewpoints of the relationship between GP and medium field models (Heisenberg model, Ising model, critical ternary medium field model, etc.), as well as the improvement of the thermal magnetic parameters when the material has GP. The magnitude of the MCE strongly depends on the essence of the phase transition and the essence of the ferromagnetic interactions in the manganites. Since the discovery of GP in magnetic materials, a number of studies have argued that the CMR effect should be seen in the context of Griffith's singularity; nevertheless, other publications have shown that GP need not be connected to the CMR in the electron-doped manganites. The huge magnetoresistive effect may exist even in the absence of a Griffiths phase, although this is an unanswered subject.

The work of Gu et al., Gordon et al., and Salamon et al. suggests that the formation of random clusters above T_C leads to Griffith's singularity and accounts for "the missing entropy". However, many recent studies suggest that the appearance of GP has enhanced the magnetocaloric effect due to the strong competition of magnetic phases. Such competition contributes additionally to the variation in entropy, and hence the Griffiths phase is one of the causes of strong MCE properties.

By comparing and updating the research results of different authors, we have found the similarities and differences of those studies and explained why there are differences in the relationship between GP and theoretical models. These are important and interesting contents that show the complex relationship of GP with other physical properties of manganites. The present discovery is of great significance because it would arouse new interest in manganites to investigate the role of the GP regime and structural distortion on turbulent physical properties such as the MR effect, MCE, thermoelectric effect, and photoelectricity. Tuning GP would become a new direction for the practical application of manganites.

CHAPTER 3. EXPERIMENTAL

The experimental approach is used in this dissertation, and data are analyzed using several theoretical models. The solid-state reaction and the sol-gel technique are discussed in this chapter. The following model systems were employed in the thesis:

The Nanocrystalline $\text{La}_{1-x}\text{Ca}_x\text{MnO}_3$ ($x = 0.20, 0.22$ and 0.25) samples were synthesized by the sol-gel process, which helped to study the effect of particle size on the appearance of GP and the relationship between GP (if any) with the MCE effect and the para-phase transition parameters of the material. The $\text{La}_{0.7}\text{Sr}_{0.3}\text{Mn}_{1-x}\text{Cu}_x\text{O}_3$ ($x = 0, 0.02, 0.04, 0.06, 0.08$ and 0.12) sample system and the $\text{La}_{0.7}\text{Sr}_{0.3}\text{Mn}_{1-x}\text{Co}_x\text{O}_3$ ($x = 0, 0.5, 0.7, 0.75, 0.8, 0.85, 0.95$ and 1) sample system were prepared by the solid phase reaction

method, which helps to investigate the influence of transition metal ions on the appearance of GP and the relationship between GP (if any) with the MCE effect and para-phase transition parameters of materials.

The structural analysis, elemental determination, and magnetic measurements have been effectively exploited to assess the quality of the material. The phase identification and structural analysis were performed by powder X-ray diffraction (XRD) using CuK α radiation ($k = 1.5406 \text{ \AA}$) at room temperature. The structural refinement was carried out by the Rietveld analysis of the X-ray powder diffraction data with the help of FULLPROF software. The surface morphology of the samples was observed using field emission scanning electron microscopy (FE-SEM, Hitachi S-4800). The elemental analysis of the samples was carried out using energy dispersive X-ray spectroscopy (EDX) coupled with a SEM instrument. The vibrating sample magnetometer (VSM) is used for investigating the magnetic properties of materials. The magnetic characterizations were performed on a Quantum Design PPMS-6000. The temperature dependence of the field-cooled (FC) and zero-field-cooled (ZFC) magnetization was recorded in various magnetic fields of 10 Oe–10 kOe.

CHAPTER 4. STUDY OF MAGNETIC PROPERTIES, MAGNETOCALORIC EFFECT AND CRITICAL EXPONENTS IN NANO $\text{La}_{1-x}\text{Ca}_x\text{MnO}_3$ ($x = 0.20, 0.22$ AND 0.25) SYSTEM

4.1. Features of structure and crystal size of the nanomaterial $\text{La}_{1-x}\text{Ca}_x\text{MnO}_3$ system

The nanocrystalline samples of $\text{La}_{1-x}\text{Ca}_x\text{MnO}_3$ ($x = 0.20, 0.22$ and 0.25) were prepared by the sol-gel process. The samples are denoted by $x = 0.2$, $x = 0.22$ and $x = 0.2$, $x = 0.22$ respectively, corresponding to the concentration of Ca in the sample of 20%; 22% and 25%.

Fig. 1 presents the powder XRD patterns and the Rietveld refinement XRD profile of $\text{La}_{1-x}\text{Ca}_x\text{MnO}_3$ ($x = 0.20, 0.22$ and 0.25) samples collected at room temperature. The analyzed data showed that the sample crystallized in an orthorhombic structure with a Pnma space group. The refined crystal structure is given in detail in Table 4.1.

The average size of the sample particles is determined using Scanning Electron Microscope (SEM) images by finding the minimum and maximum sizes of the large number of particles (seen in Fig. 4.2). It can be evidently seen from particle size distribution histograms that the average particle size of $\text{La}_{1-x}\text{Ca}_x\text{MnO}_3$ samples

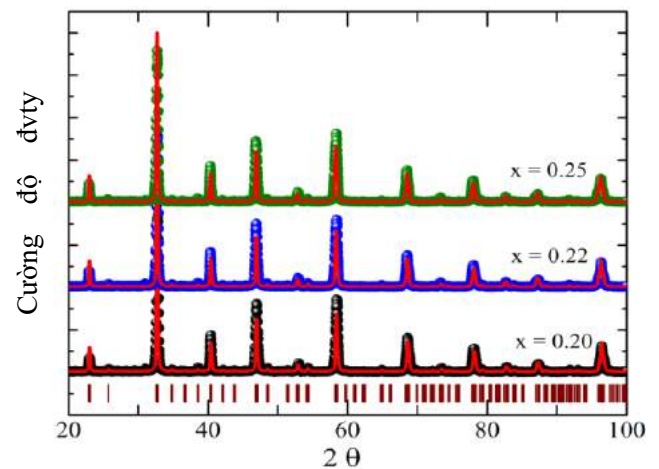


Fig. 4.1. Refined X-ray powder diffraction patterns of the nanocrystalline $\text{La}_{1-x}\text{Ca}_x\text{MnO}_3$ ($x = 0.20, 0.22$, and 0.25) samples.

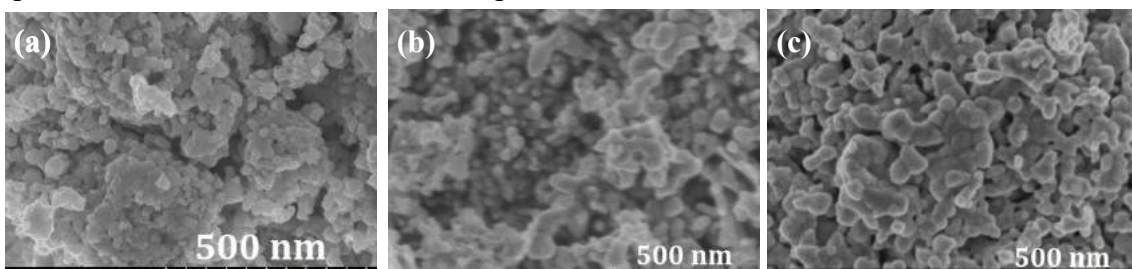


Fig. 4.2. Field emission scanning electron microscope (FESEM) images of $\text{La}_{1-x}\text{Ca}_x\text{MnO}_3$ samples with $x = 0.20$ (a), $x = 0.22$ (b), $x = 0.25$ (c).

with concentrations of $x = 0.20$, $x = 0.22$, and $x = 0.25$ is estimated to be 60, 90, and 80 μm , respectively. The grain size obtained by SEM is larger than that calculated by Scherrer's formula. This can be explained by the fact that each particle observed by SEM consists of several crystallized grains. Besides that, EDX analysis was performed on the sample, and all peaks were labeled with their constituent elements. The values of atomic percentage obtained from EDX measurements are nearly equal to their corresponding stoichiometric values. This fact indicates that there is no loss of any element during sintering.

Table 4.1. Refined structural parameters of the nano $\text{La}_{1-x}\text{Ca}_x\text{MnO}_3$ ($x = 0.20, 0.22, \text{ and } 0.25$) system at room temperature.

Parameters	$x = 0,20$	$x = 0,22$	$x = 0,25$
Space group	<i>Pnma</i>	<i>Pnma</i>	<i>Pnma</i>
a (Å)	5,4761	5,4671	5,4609
b (Å)	7,4794	7,7171	7,7195
c (Å)	5,4968	5,488	5,4730
V (Å ³)	233,26	231,54	230,72
$\langle\text{Mn-O}\rangle$ (Å)	1,959	1,963	1,959
$\langle\text{Mn-O-Mn}\rangle$ (°)	161,9	160,5	161,6
D_{XRD} (nm)	30	50	40
D_{SEM} (nm)	60	90	80
$\langle W \rangle$	0,0937	0,0931	0,0938

4.2. Characteristics of Griffith phase in nanomaterial $\text{La}_{1-x}\text{Ca}_x\text{MnO}_3$ ($x = 0.20; 0.22$ and 0.25)

The magnetization as a function of temperature $M(T)$ for $\text{La}_{1-x}\text{Ca}_x\text{MnO}_3$ ($x = 0.20, 0.22, \text{ and } 0.25$) samples was measured under a 50 Oe field, as shown in Figs. 4.4(a)–4.4(c). The Curie temperature (T_C) of ($x = 0.20; 0.22; \text{ and } 0.25$) samples, determined at the minimum of dM/dT versus T curves (see inset of Fig. 4.4), is found to be 214 K, 138.5 K, and 222 K, respectively. It should be noticed that the T_C values of $x = 0.20$ and 0.25 samples are much higher than the reported T_C values of polycrystalline bulk samples (specifically $x = 0.20$ (183 K) and $x = 0.25$ (177 K) with the same composition). Meanwhile, the T_C values of the $x = 0.20$ sample (138.5 K) are much smaller than the reported T_C value of the polycrystalline bulk $\text{La}_{0,78}\text{Ca}_{0,22}\text{MnO}_3$ sample (189 K). The T_C temperature in our samples varies non-linearly, in contrast to the phase diagram of the $\text{La}_{1-x}\text{Ca}_x\text{MnO}_3$ system.

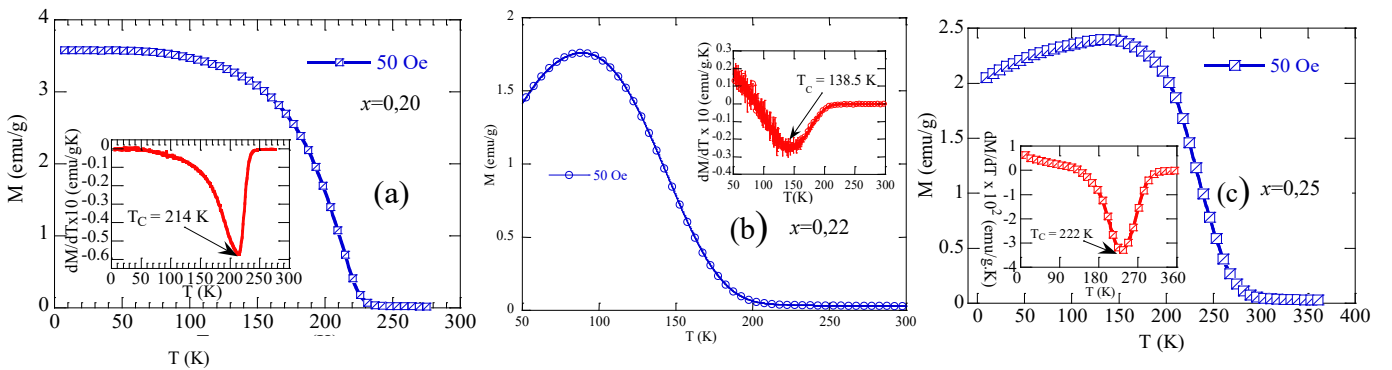


Fig. 4.4. Temperature dependence of magnetization in the *FC* mode under a 50 Oe applied field for $x = 0.20$ (a), $x = 0.22$ (b), and $x = 0.25$ (c) samples. Inset the dM/dT vs. T curves.

Fig. 4.5 represents the plot of the inverse of the susceptibility $\chi^{-1}(T)$ (defined as $\chi^{-1} = H/M$ of $x = 0.20, 0.22, \text{ and } 0.25$ samples, respectively) versus temperature for the samples in a magnetic field of 50 Oe and its linear fit to the Curie-Weis law. As can be seen in the figure, the downturn in the $\chi^{-1}(T)$ at temperatures above T_C is indicative of the existence of the Griffiths phase or magnetic polarons in the paramagnetic phase.

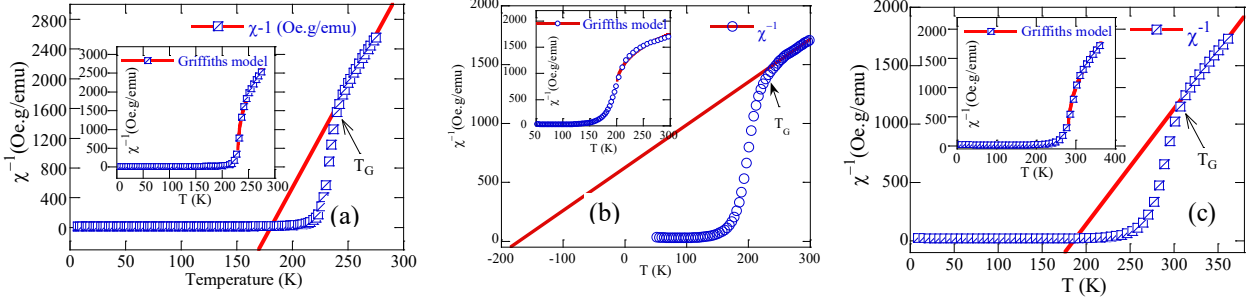


Fig. 4.5. Variation of the inverse of the susceptibility ($1/\chi$) with temperature for $x = 0.20$, $x = 0.22$, and $x = 0.25$ samples at $H = 50$ Oe. The straight, solid line indicates the best fit of the Curie-Weiss law in the paramagnetic range ($T > T_G$). The solid lines in the inset are the fit with the power law equation (1.4) $\chi^{-1}(T) \sim (T - T_C^{Rand})^{1-\lambda_{GP}}$ ($0 < \lambda_{GP} < 1$).

This behavior can also be understood and explained by the scenario of the phase competition between the FM metallic phase and an antiferromagnetic (AFM) insulating phase, as figured out in recent experiments and theories. The temperature corresponding to the onset of the downturn (i.e., the temperature where $\chi^{-1}(T)$ deviates from the linear behavior of the Curie-Weiss law in the paramagnetic region, which is indicative of the existence of the Griffiths phase or magnetic polarons in the paramagnetic phase. Therefore, this behavior can be understood and explained by scenarios of phase separation. The Griffiths temperature T_G is defined as the onset of the downturn (see Fig. 4.5), which are found to be 240 K, 200 K and 296 K for $x = 0.20$ (a), $x = 0.22$ (b) and $x = 0.25$ (c), respectively. The Curie - Weiss temperatures (θ_{cw}) are seen to be 180 K, -193 K, and 186 K, for $x = 0.20$, 0.22, and 0.25, respectively, by fitting the data in the PM region. The positive value of θ_{cw} for $x = 0.20$, 0.25 confirms the presence of FM interactions below the Curie temperature. The negative value of θ_{cw} of the sample $x = 0.22$ indicates that the cause of the magnetic abnormality of the same sample may be that it is different from the other two samples. The negative value of θ_{cw} of the sample $x = 0.22$ indicates that the cause of the magnetic abnormality of the sample may be different from the other two samples. Therefore, to explain exactly the cause of this strange magnetic phase formation, we first use the GP model to find the characteristic parameters and compare them with the theory.

Table 4.2. Magnetic data of the nano $\text{La}_{1-x}\text{Ca}_x\text{MnO}_3$ ($x = 0.20, 0.22, \text{ and } 0.25$) system. The experimental effective paramagnetic moment μ_{eff}^{exp} , the theoretical effective paramagnetic moment μ_{eff}^{theo} ; T_C is the Curie temperature, C is the Curie constant and θ_{cw} (K) refers to Weiss temperature. The parameters evaluated from Griffiths model: T_C^{Rand} ; T_G ; λ_{GP} .

Parameters	$x = 0.20$ $H=50$ Oe	$x=0.22$ $H=50$ Oe	$x = 0.25$ $H= 50$ Oe
T_C (K)	214	138,5	222
θ_p (K)	180	-193	186
$C \times 10^2$ (emu.K/Oe.g)	3.66	30,2	10.09
μ_{eff}^{exp} (μ_B)	8.07	23.05	13.24
μ_{eff}^{theo} (μ_B)	4.71	4.69	4.66
T_G (K)	240	201	296
T_C^{Rand} (K)	230	196	280
λ_{GP}	0.63	0.77	0.60

It has been shown that the Griffiths phase is unequivocally characterized by a magnetic susceptibility exponent between 0 and 1; that is: $\chi^{-1}(T) \sim (T - T_C^{Rand})^{1-\lambda_{GP}}$ ($0 < \lambda_{GP} < 1$)

The red solid line in the inset of Fig. 4.5 is the fit with Eq. (1.4), and the corresponding fitting parameter is the disorder - dependent FM ordering temperature (T_C^{Rand}); the Griffiths temperature (T_G), the Griffiths exponent λ_{GP} of samples are given in Table 4.2. Value of $\lambda_{GP} = 0.63$; 0.77 and 0.6 , respectively, for the samples $x = 0.20$, $x = 0.22$, and $x = 0.25$, which are consistent with the condition that Griffith phase appears in the manganites.

We calculated the experimental effective paramagnetic moment (μ_{eff}^{exp}) using the determined Curie constant (C) according to the following relation (1.4). The theoretical effective paramagnetic moment μ_{eff}^{theo} is given by Equation (1.3). The values of the μ_{eff}^{theo} and the μ_{eff}^{exp} for the three samples are reported in Table 4.2. Comparing these two values, it can be seen that they satisfy the (iv) criterion of GP occurrence. According to the characteristics of GP, a much larger effective spin proves the presence of GP in our sample.

To get an accurate conclusion about the GP appearance in the sample, we surveyed the saturation magnetic moment of all three samples (theoretical and experimental) from the magnetization curve at 5 K in the 5 T magnetic field. Figure 4.6 shows the magnetization curves of the three samples and how they are determined from their experimental saturation. The obtained values were 80.5 emu/g, 35.2 emu/g, and 59.2 emu/g for samples $x = 0.20$, $x = 0.22$, and $x = 0.25$, respectively.

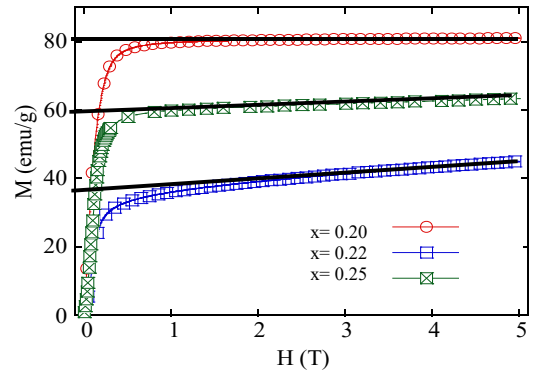


Fig. 4.6. Isothermal magnetization curve of three samples in a 5 T magnetic field.

From the above results, we calculated the magnetic moment of saturation. The results of the 3 samples were $3.18 \mu_B$, $1.38 \mu_B$, and $2.29 \mu_B$ for the samples $x = 0.20$, $x = 0.22$, and $x = 0.25$, respectively. From this, we infer that the values for $x = 0.20$, $x = 0.22$, and $x = 0.25$ are $3.8 \mu_B$, $3.78 \mu_B$, and $3.75 \mu_B$, respectively. These results are greater than the evidence that there is no spin-orbit coupling in the samples. Thus, quenching of spin-orbit coupling is the main cause of the appearance of GP in all three samples.

One of the basic features of GP is the existence of ferromagnetic clusters of finite size and the absence of spontaneous magnetization and long-range FM ordering, so in the region $T_C < T < T_G$, the spontaneous magnetization of the material $M_{spont} = 0$. This can be seen in Figure 4.8. This feature once again confirms that this is the GP in all three of our models.

In order to demonstrate the hypothesis that the Griffiths-like phase is present in our sample, we

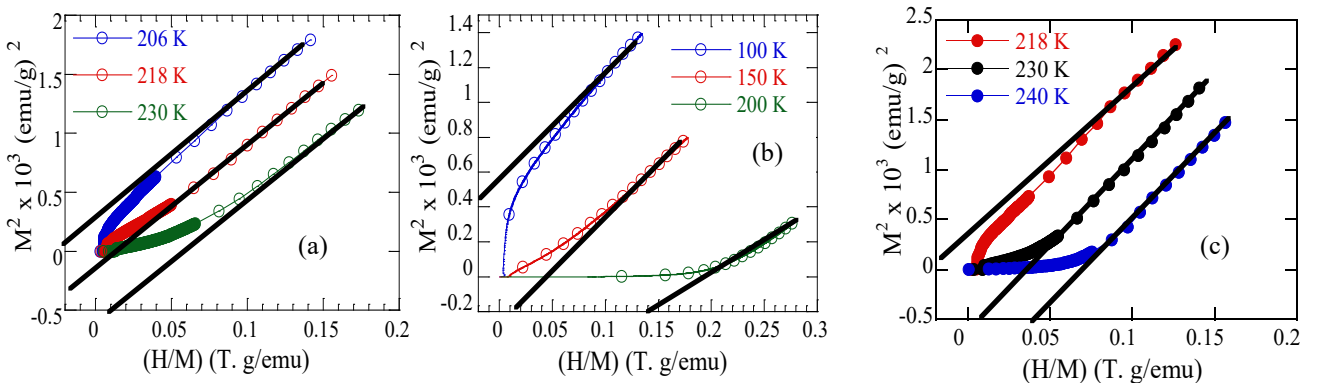


Fig. 4.8. Arrott plots in the $T_C < T < T_G$ region for $x = 0.20$ (a), $x = 0.22$ (b), and $x = 0.25$ (c) samples. The solid line is a linear extrapolation.

further investigated the evolution of Griffiths-like phases as a function of external fields.

Fig. 4.9 represents the plot of the inverse of the susceptibility versus temperature for $x = 0.20$ and $x = 0.25$ samples in different magnetic fields. As shown in Fig. 4.9, $\chi^{-1}(T)$ sharply deviates downward from the Curie – Weiss behavior under the lower magnetic fields below T_G , and the deviation becomes negligible at higher magnetic fields such as $H = 10$ kOe. This shows that when increasing the magnetic field strength, the anomalous state in the paramagnetic region of the sample is gradually broken, and this state is completely extinguished when the magnetic field is large enough. This result may be attributed to the polarization of spins outside the clusters, which, therefore, leads us to expect the presence of the GP.

However, the experimental effective paramagnetic moment of the $x = 0.20$ sample does not completely satisfy the GP criterion; therefore, in order to get further insight into the effect of disorder on the nature of GP, we have used the theoretical formula of Galistski et al. According to the formula, the magnetization of the GP depends on the temperature and magnetic field: $M(H,T) \sim \exp[-C(T/H)]$ (4.5). Where the constant C is proportional to the sum of the magnetic moments of a ferromagnetically ordered cluster. Above T_C , the magnetization of the $x = 0.20$ sample excellently fits the equation (4.5) for $H = 1$ kOe and $H = 10$ kOe and is shown in Fig. 4.10. From the fit, C is estimated to be 0.283×10^{-3} kOe/K, 0.587×10^{-3} kOe/K and 0.989×10^{-3} kOe/K for $H = 50$ Oe, $H = 1$ kOe, and $H = 10$ kOe, respectively. On the other hand, it can be seen that the magnetic moment decreases gradually as the magnetic field increases, due to the strengthening of the paramagnetic background in this region. Thus, this does not only confirm the increase in cluster size with the magnetic field but also indicate the consistency in the Griffith phase behavior with the increased applied field.

Additionally, it was predicted by Saha in their theoretical calculations on GP that all the magnetization derivatives with respect to field (the peak of dM/dH) above T_C are finite at $H = 0$ for a GP system, but the nonlinear relationship between dM/dH and the magnetic field is still observed. Hence, the observed uprise at the lower field region for the temperature range $T_C < T$

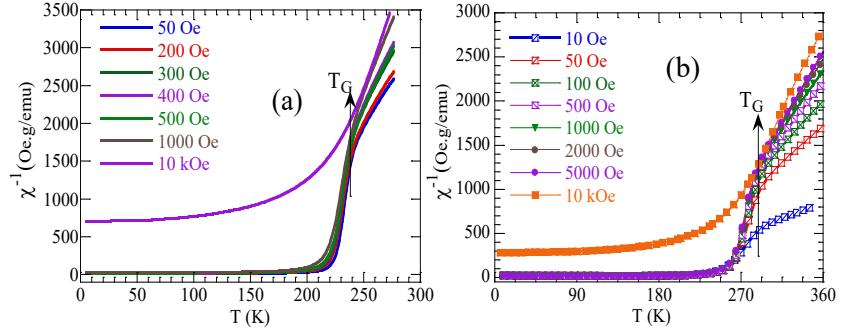


Fig. 4.9. Temperature dependencies of the inverse susceptibility under different magnetic fields for $x = 0.20$ (a) and $x = 0.25$ (b) samples.

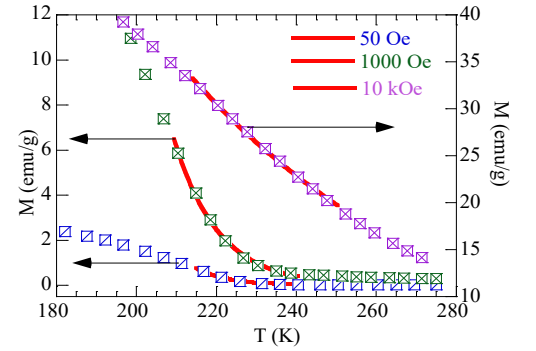


Fig. 4.10. An equation of $M(H,T) \propto \exp[-C(T/H)]$ is used to fit the $M(T)$ curves in a field of 50 Oe, 1 kOe, and 10 kOe for the $x = 0.20$ sample.

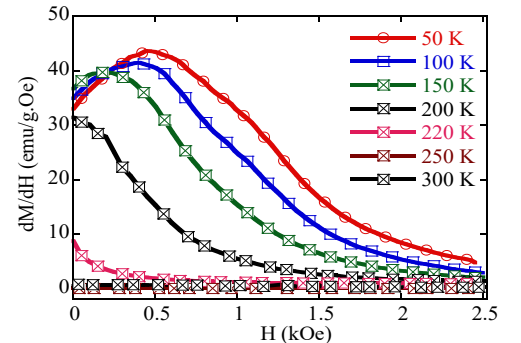


Fig. 4.11. dM/dH (M is initial magnetization) versus H at different temperatures both below and above T_C for $x = 0.20$ representative samples.

$< T_G$ in Fig. 4.11 supports the theoretical prediction. This result is another important proof that GP is present in $x = 0.20$.

For a more in-depth conclusion on GP occurrence in the samples, it is important to investigate the effect of surface pressure as the particle size reduction that acts as a driving force for the GP to emerge in the system. The calculated orthorhombic distortions, i.e., strain field parameters, for three samples are $OS_{//} = 0.309, 0.341, \text{ and } 0.343$ and $OS_{\perp} = 1.077, 1.090, \text{ and } 1.092$. The presence of strain fields in such types of nanomaterials ruffles the Mn-O-Mn network, and the small difference between in-plane ($OS_{//}$) and out-of-plane (OS_{\perp}) strain fields tries to freeze the small FM clusters in the core. The stable state of the GP in the PM region can also be clearly explained using an energy diagram.

The pinning potential barrier can be easily calculated $U \sim k_B T_G$. The values come out to be 21 meV, 17 meV, and 25 meV for $x = 0.20, x = 0.22, \text{ and } x = 0.25$, respectively. The calculated magnetic energy (E_{mag}) owing to the formation of FM clusters in the GP region for the application of $H = 10$ kOe is ~ 3 meV. Therefore, $E_{\text{mag}} < U$, but the energy involved for the surface pressure (~ 54 meV) is high. Thus, the FM clusters get pinned in the system, and it needs ~ 30 meV of thermal energy to reach the pure PM region. Hence, the existing strain fields due to the surface pressure effect at the GP region can be the source, which prevents the FM clusters from reaching the PM state immediately above the T_C . Thus, the energy diagram explains well the origin of GP as well as its stability in the PM region in the $\text{La}_{1-x}\text{Ca}_x\text{MnO}_3$ system.

Thus, we demonstrated the presence of Griffiths in the samples, the cause of Griffith phase emergence from competition of ferromagnetic and antiferromagnetic interactions, and the quenching of spin-orbit bonds in the material. The Griffiths phase in the samples $\text{La}_{0.75}\text{Ca}_{0.25}\text{MnO}_3$ and $\text{La}_{0.8}\text{Ca}_{0.2}\text{MnO}_3$ completely disappeared in the 10 kOe magnetic field. The role of the non-magnetic shell in GP formation has been analyzed and interpreted based on empirical evidence.

4.3. Critical exponents of $\text{La}_{1-x}\text{Ca}_x\text{MnO}_3$ ($x = 0.20$ and 0.25) nanoparticles

In this section, we explain the relationship between the Griffiths phase and the phase transition parameters in $\text{La}_{0.75}\text{Ca}_{0.25}\text{MnO}_3$ nanoparticles and $\text{La}_{0.8}\text{Ca}_{0.2}\text{MnO}_3$ nanoparticles.

To get more insight into the phase-transition type and magnetic interactions of samples, we use the $M(H, T)$ data of the samples $x = 0.20$ and $x = 0.25$ to construct the Arrott plot. The sign of the slope of the Arrott plot gives information related to the order of the phase transition; the negative slope corresponds to the first-order magnetic transition and the positive to the second-order (SOMT) one. The results show that all the M^2 vs. H/M curves exhibit a positive slope, indicating this sample is characterized by a SOMT.

This result shows that the critical exponents found by different methods are close to each other. The exponent values found are close to those expected by the mean-field model. And, therefore, it is plausible that the critical exponents in samples could be related to the long-range FM interactions in which they approach the mean field values. In this case, the formation of GP in the sample is perhaps the main factor in the occurrence of the long-range interaction.

To supplement the assessment of the accuracy of the critical exponents of the material as well as the role of GP on these parameters, we used the re-normalization group theory of Fisher et al. The values of other reduction parameters, such as $\nu = \gamma/\sigma$, β/ν are calculated and compared with the theoretical models as shown in Table 4.5. The values of the critical parameters do not belong to any universal model, so we went on to use Suzuki's model, which, instead of considering the temperature difference of the

exponents, investigated the correlation length $\xi(T) \approx |T_C - T|^{-\nu}$ (4.10) with respect to temperature, which corresponds to different values of, here related via the “length exponent” by the formula $\nu = \gamma/\sigma$.

We have shown in Fig. 4.5 that it can be seen that the reduced parameters do not completely coincide with any theoretical model, so it is likely that another value of the correlation length exists in the sample. Therefore, it can be concluded that internal disorders and non-homogeneous states are present in $x = 0.20$ and $x = 0.25$. The presence of these states is a prerequisite for the appearance of GP in the system, as indicated

Table 4.5. The reduced exponents of $x = 0.20$ and $x = 0.25$ samples and the various theoretical models.

Sample	d	n	σ	theoretical model	$\nu = \frac{\gamma}{\sigma}$	$\frac{\beta}{\nu}$	$\frac{\gamma}{\nu}$
$x = 0.20$	3	1	1.509		0.665	0.795	1.509
		2	1.507		0.666	0.794	1.507
		3	1.507		0.666	0.794	1.507
		∞	1.503		0.668	0.792	1.564
$x = 0.25$	3	1	1.344		0.699	0.757	1.344
		2	1.371		0.686	0.771	1.371
		3	1.388		0.677	0.781	1.388
		∞	1.454		0.646	0.819	1.454
				MFT	0.5	1	2
				3D-Ising	0.63	0.516	1.969
				3D-XY	0.67	0.515	1.964
				3D-Heisenberg	0.705	0.518	1.966
				Spherical symmetry	1	0.5	2

in previous studies. This is also evidenced by the phase transition width indicated in the samples, where the minimum of dM/dT is in a wide range and not as sharp as conventional block samples.

Usually, the appearance of the Griffiths phase associated with short-range interactions with the 3D-Ising model is observed. However, it can be seen that the critical exponents of the nano $\text{La}_{1-x}\text{Ca}_x\text{MnO}_3$ ($x = 0.20, 0.22,$ and 0.25) sample are close to those of the mean-field model. This proves the presence of long-range magnetic order in the sample. This is in line with recent GP studies, which propose that in order for the Griffiths phase to occur, the system must closely follow a certain universal phase transition model rather than necessarily the classic Ising model.

4.5. The magnetocaloric effect in $\text{La}_{1-x}\text{Ca}_x\text{MnO}_3$ ($x = 0.20$ and 0.25) nanoparticles

The magnetocaloric effect in $\text{La}_{1-x}\text{Ca}_x\text{MnO}_3$ ($x = 0.20$ and 0.25) nanoparticles has been studied in detail in relation to GP and particle size effects.

4.5.1. The magnetocaloric effect in $\text{La}_{0.75}\text{Ca}_{0.25}\text{MnO}_3$ nanoparticles

In this part, together with assessing the critical behaviors for the $\text{La}_{0.75}\text{Ca}_{0.25}\text{MnO}_3$ sample, we also considered the magnetic entropy change $\Delta S_M(T)$ and its field dependence, as shown in Fig. 4.22. At a given temperature, $\Delta S_M(T)$ increases with increasing H . At a given magnetic field, $\Delta S_M(T)$ is maximized near at T_C . For example, the maximum value of $\Delta S_M(T)$, $|\Delta S_M^{max}| = 2 \text{ J/kg}\cdot\text{K}$, is about $1.9 \text{ J/kg}\cdot\text{K}$ in the field $H = 2 \text{ T}$, which is close to that obtained for the same compound ($|\Delta S_M^{max}| = 2 \text{ J/kg}\cdot\text{K}$ in $\Delta H = 1.5 \text{ T}$) by Guo et al. Thus, the appearance of GP in the material has

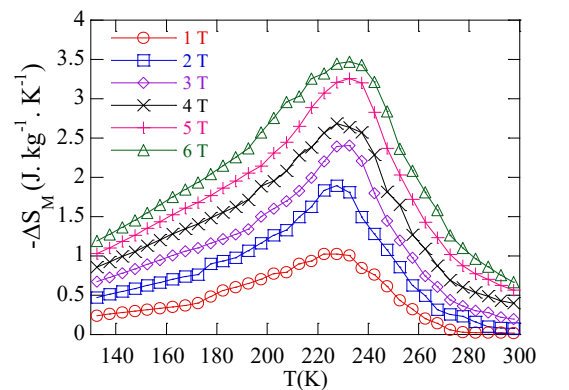


Fig. 4.22. Magnetic entropy change ΔS_M vs. the temperature of the $x = 0.25$ sample under different magnetic field strengths (1, 2, 3, 4, 5, and 6 T).

significantly affected $|\Delta S_M^{max}|$. In the case of materials with GP, due to the appearance of FM clusters in the paramagnetic zone, when the material is magnetized, it is possible that the sudden decrease from the degree at the nearby Curie temperature (from the ferromagnetic to the paramagnetic zone) is not as favorable as in the case of materials with only the paramagnetic phase below the Curie temperature, so the magnetic entropy change cannot be as high as desired.

Figure 4.23 shows the magnetic entropy change according to the magnetic field at temperatures above and below T_G . Obviously, we can only observe that the relationship occurs in the region on T_G (pure paramagnetic region), while in the $T_C < T < T_G$ region, this relationship is unsatisfactory, meaning that there are iron interactions at short distances. In addition, it should be noted that the linear increase of ΔS_M the magnetic field in this area is because the magnetic level does not reach the saturation value right in the high magnetic field. Thus, GP may be the reason for the existence of magnetic entropy variation in the wide temperature range up to and in the larger magnetic field due to GP disappearance and the asymmetry of the reduction.

4.5.1. The magnetocaloric effect in $\text{La}_{0.78}\text{Ca}_{0.22}\text{MnO}_3$ nanoparticles

The magnetic entropy change of the $x = 0.22$ sample was calculated using the phenomenological model from the temperature dependence of the magnetization $M(T)$ data of the sample. The variation in ΔS_M with temperature under the different applied magnetic fields for the $x = 0.22$ sample is shown in Fig. 4.7. The maximum magnetic entropy change was found to be 0.95 J/kg.K for $H = 12 \text{ kOe}$, making this material a suitable candidate for magnetic refrigeration applications.

Usually, the large change in magnetic entropy variation in manganites is derived from the sudden change of magnetic gradients around T_C . Similar to the $x = 0.22$ sample, the appearance of GP in the paramagnetic region can reduce this abrupt change, so the magnitude of the change will be affected. However, in this case, because the occurrence of the AFM phase is stronger than that of the $x = 0.25$ sample, the large value of it can be compared with other bulk materials.

The Griffith phase affected the magnetic properties of $\text{La}_{0.78}\text{Ca}_{0.22}\text{MnO}_3$ materials and enhanced the values of magnetic entropy and thermal capacity variations of the materials. This has many implications for the application of materials to magnetic refrigeration techniques.

Thus, in the case of the sample $\text{La}_{0.75}\text{Ca}_{0.25}\text{MnO}_3$, the magnetic entropy variation is not significant compared to the highest value recently achieved in this material. This is because the occurrence of a neighboring FM phase under T_C makes the variation of the magnetic temperature under the neighboring temperature T_C not as high as expected, whereas the occurrence of a strong antiferromagnetic interaction in the

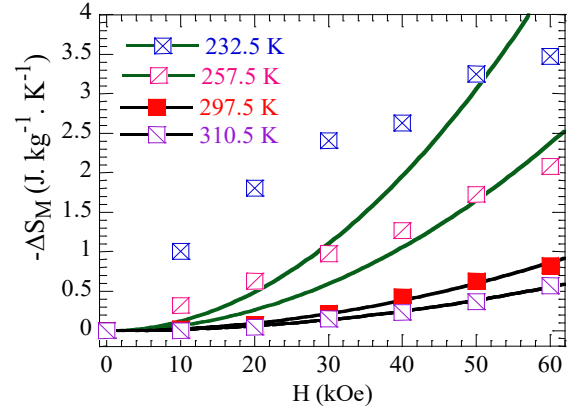


Fig. 4.23. The magnetic field dependence of the magnetic entropy variation of $x = 0.25$ at temperatures in the upper and lower regions T_G .

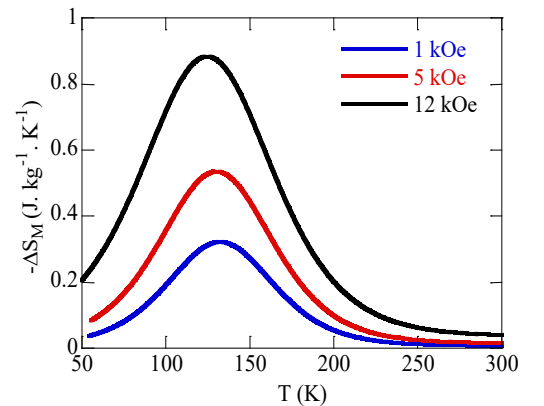


Fig. 4.27. Temperature dependence of ΔS_M under different applied fields for a $\text{La}_{0.78}\text{Ca}_{0.22}\text{MnO}_3$ sample under different applied magnetic fields (1, 5, and 12 kOe).

material $\text{La}_{0.78}\text{Ca}_{0.22}\text{MnO}_3$ gives a greater magnetic entropy variation in this material.

4.6. Phase diagram of $\text{La}_{1-x}\text{Ca}_x\text{MnO}_3$ system ($x = 0.20$; $x = 0.22$ and $x = 0.25$)

According to the phase diagram for the $\text{La}_{1-x}\text{Ca}_x\text{MnO}_3$ system's GP phase, no GP occurs at concentrations of $x = 0.2$ and occurs instead in the range 0.18 to 0.33. When the concentration of x is raised from 0.18 to 0.25, we can also see a tendency for the distance between T_C and T_G to close. When Ca doping is elevated to "optimal" levels at doping concentration $x = 0.33$, this narrowing is accelerated. When Ca doping is elevated to "optimal" levels at doping concentration $x = 0.33$, this narrowing is accelerated. However, our results show that at the concentration $x = 0.2$, GP appears, and there is an expansion of the distance between T_C and T_G on the phase diagram corresponding to an increase in the doped concentration from 0.2 to 0.25 in the $\text{La}_{1-x}\text{Ca}_x\text{MnO}_3$ nanosystem (Figure 4.30). As analyzed above, the quenching of spin-orbit coupling interaction and the role of the shell have caused GP to appear in the $\text{La}_{1-x}\text{Ca}_x\text{MnO}_3$ nanosystem, especially GP to appear immediately at the concentration $x = 0.20$, contrary to observations in the bulk sample.

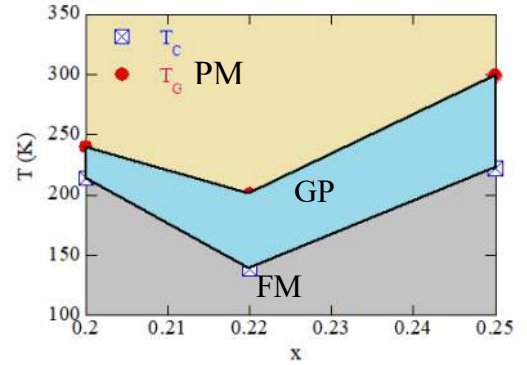


Fig. 4.30. GP appearance diagram for $\text{La}_{1-x}\text{Ca}_x\text{MnO}_3$ ($x = 0.20$; $x = 0.22$ and $x = 0.25$) system.

CHAPTER 5. EFFECTS OF Cu ION SUBSTITUTION ON MAGNETIC PROPERTIES, PHASE TRANSITION PROPERTIES, MAGNETOCALORIC EFFECTS, AND GRIFFITH PHASE IN THE MATERIAL $\text{La}_{0.7}\text{Sr}_{0.3}\text{Mn}_{1-x}\text{Cu}_x\text{O}_3$ SYSTEM AND EFFECT OF CO ION SUBSTITUTION ON MAGNETIC PROPERTIES, GRIFFITH PHASE IN MATERIAL $\text{La}_{0.7}\text{Sr}_{0.3}\text{Mn}_{1-x}\text{Co}_x\text{O}_3$ SYSTEM

The effects of Cu non-magnetic ions and Co magnetic ions substituting Mn on the structure, magnetic properties, magnetocaloric behavior, critical behavior, and Griffith phase in $\text{La}_{0.7}\text{Sr}_{0.3}\text{Mn}_{1-x}\text{M}_x\text{O}_3$ ($M = \text{Cu}$ và Co) have been meticulously examined in detail in this chapter.

5.1. Structure and magnetic properties of the $\text{La}_{0.7}\text{Sr}_{0.3}\text{Mn}_{1-x}\text{Cu}_x\text{O}_3$ ($x = 0.02, 0.04, 0.06, 0.08,$ and 0.12) system

5.1.1. Effect of Cu ion substitution on the structure of $\text{La}_{0.7}\text{Sr}_{0.3}\text{Mn}_{1-x}\text{Cu}_x\text{O}_3$ ($x = 0.02, 0.04, 0.06, 0.08,$ and 0.12) system

Figures 5.1 and 5.2 present the XRD patterns and the results of Rietveld analysis of samples prepared by the solid-state reaction method. In comparison with the crystallography library, these results suggest that the sample has a rhombohedral structure with a space group $R\bar{3}c$. Samples $x = 0.02$; $x = 0.04$, and $x = 0.06$ (Figure 5.1) neither observed strange peaks nor similar lattice parameters obtained by other authors, which confirm that the Cu atoms have been replaced in the position of Mn (position 6e) of the lattice.

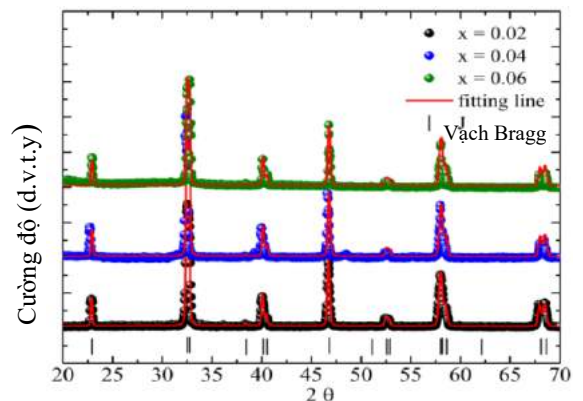


Fig. 5.1. The XRD analysis along with Rietveld refinement for $x = 0.02$, $x = 0.04$, and $x = 0.06$ samples.

However, Mn_3O_4 minor phases appeared in both samples with $x = 0.08$ and $x = 0.12$, as shown in Figure 5.2. Mn_3O_4 is nonmagnetic, and its amount is negligible; thus, these compounds do not influence the magnetic properties of the host samples. From Fig. 5.2, no shift in the characteristic rhombohedral peaks is observed with increasing Cu doping. Therefore, no stress exists in either sample, and local structural distortions are minimized.

Lattice parameters, unit cell volume, and fitting parameters are listed in Table 5.1. The rhombohedral structure of the samples remains unchanged despite increases in Cu doping content, and the corresponding structural parameters do not change significantly (see Table 5.1). When the Cu concentration increased to 12%, the unit cell volume decreased rapidly.

Table 5.1. Refined Structural Parameters, the Curie temperature (T_C), the experimental effective paramagnetic moment (μ_{eff}^{exp}) and the theoretical effective paramagnetic moment (μ_{eff}^{theo}) of the $La_{0.7}Sr_{0.3}Mn_{1-x}Cu_xO_3$ system at room temperature.

Sample	$x = 0.02$	$x = 0.04$	$x = 0.06$	$x = 0.08$	$x = 0.12$
a (Å)	5.5052	5.5056	5.5021	5.4958	5.4929
c (Å)	13.356	13.344	13.342	13.346	13.344
V (Å ³)	350.56	350.04	349.79	349.08	348.66
Mn-O (°)	170.20	169.20	169.12	168.30	167.10
Mn-O-Mn (Å)	1.940	1.945	1.946	1.948	1.949
W ($\times 10^{-2}$)	9.833	9.745	9.728	9.693	9.675
T_C (K)	360	356	357	298	297
θ_w (K)	361	357	359	357	349
μ_{eff}^{exp} (μ_B)	5.57	5.56	5.57	6.10	5.57
μ_{eff}^{theo} (μ_B)	4.59	4.55	4.52	4.49	4.43

5.1.2. Effect of Cu ion substitution on the magnetic properties of $La_{0.7}Sr_{0.3}Mn_{1-x}Cu_xO_3$ ($x = 0.02, 0.04, 0.06, 0.08, \text{ and } 0.12$) system

The effect of the substitution concentration of Cu on the magnetization of the samples shown on the temperature dependence of field - cooled (FC) magnetization ($M - T$ curves) at the magnetically applied field of 100 Oe is shown in Fig. 5.3. With samples $x = 0.02, 0.04, \text{ and } 0.06$, the magnetization decreases sharply with an increase in temperature near T_C . The inset presents the plot of dM/dT vs. T with values of 360 K, 356 K, and 357 K, respectively, which is the minimum temperature of dM/dT . Obviously, the T_C of the $x = 0.02$ sample approximates the T_C of the $x = 0.0$ (364 K) sample and decreases slowly to $x = 0.06$, then decreases rapidly as the concentration of Cu increases. The downward trend in T_C is consistent with the increase in local network distortion derived from the integral transfer between the 3d orbitals of the Mn ion and the 2p orbitals of the oxygen ion.

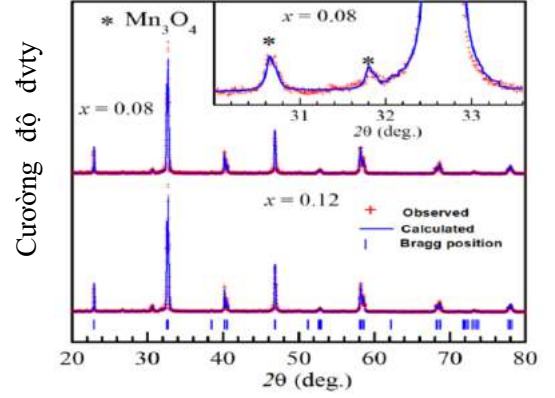


Fig. 5.2. The XRD analysis along with Rietveld refinement for $x = 0.08$ and $x = 0.12$ samples.

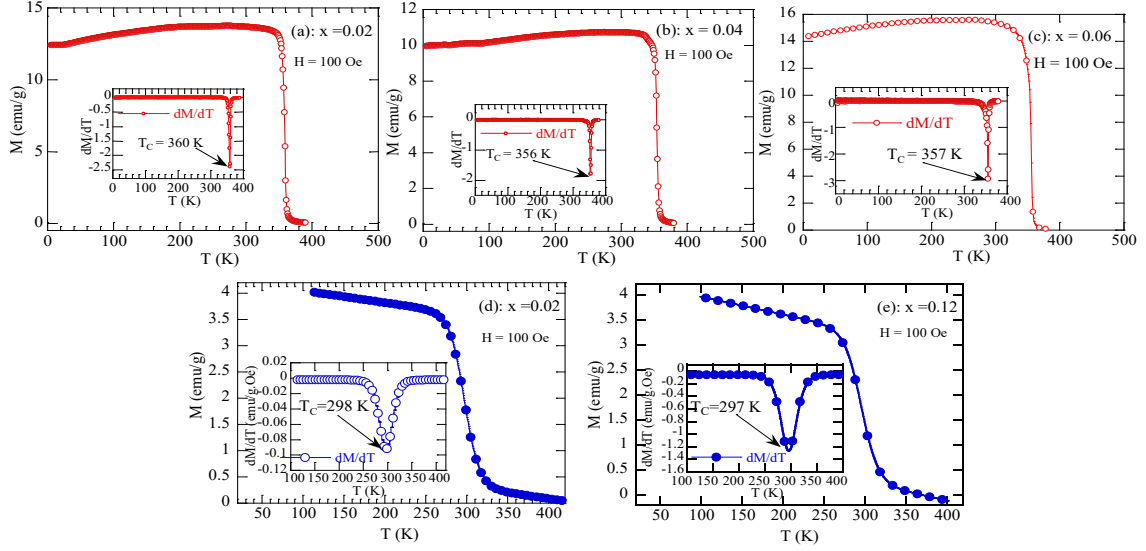


Fig. 5.3. Temperature dependence of magnetization at 100 Oe of $\text{La}_{0.7}\text{Sr}_{0.3}\text{Mn}_{1-x}\text{Cu}_x\text{O}_3$
The inset shows the dM/dT curves.

Figure 5.4 presents the temperature dependence of inverse magnetic susceptibility for all samples in a magnetic field of 100 Oe. The red line indicates the fit to the data using the Curie - Weiss law. A linear relationship clearly exists between χ^{-1} and T as expected from the Curie - Weiss equation. The Curie - Weiss temperature for samples are listed in Table 5.1; a positive value indicates that these samples are dominated by the FM exchange interaction between spins. Moreover, θ_p is higher than T_C , and this fact can be attributed to the existence of short-range FM ordering. However, these ferromagnetic phrases do not appear GP in the samples. The Griffith phase does non-formation in the $\text{La}_{0.7}\text{Sr}_{0.3}\text{Mn}_{1-x}\text{Cu}_x\text{O}_3$ system ($0 \leq x \leq 0.12$). Using least-squares fitting to obtain the value of C , the experimentally determined effective PM moment is calculated as follows Equation (1.7). We also calculated the theoretical effective moment. These values are smaller than the calculated effective PM moment. These results are attributed to the presence of Zener and the local Jahn-Teller lattice distortion (JT) occurring above the T_C temperature. In the $\text{La}_{1-x}\text{Sr}_x\text{MnO}_3$ system, Jahn-Teller (JT) distortions have been identified as the reason for the appearance of the GP. With Cu-substitution, Cu^{2+} ions exhibit a JT distortion, while

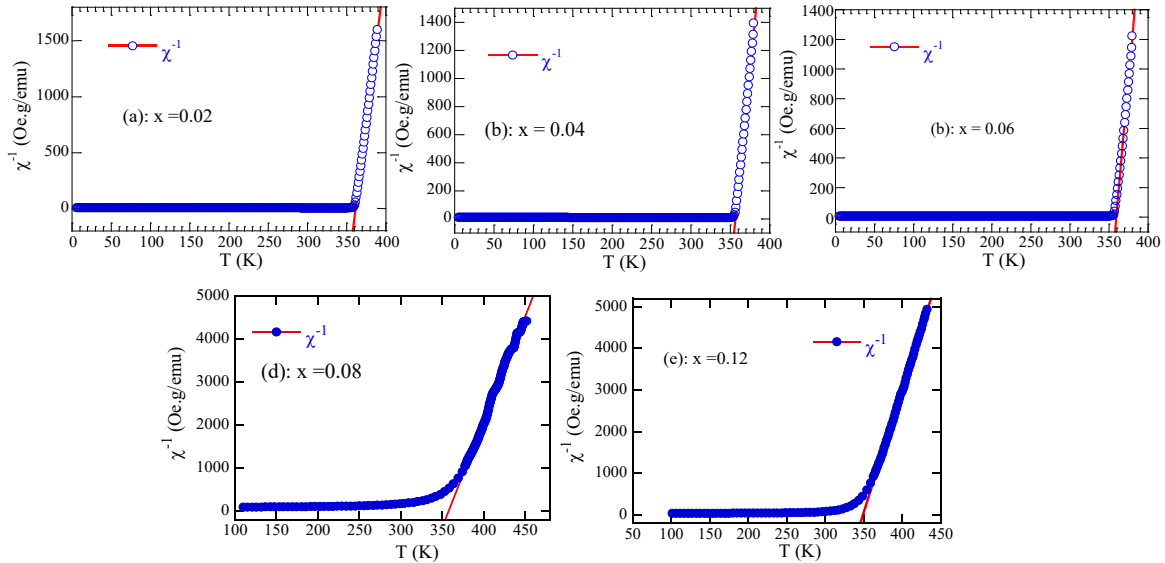


Fig. 5.4. Temperature dependence of inverse magnetic susceptibility at 100 Oe for $x = 0.02$ (a), $x = 0.04$ (b), $x = 0.06$ (c), $x = 0.08$ (d), and $x = 0.12$ (e) samples.

Cu^{3+} ions don't. From the balance of valence charges, Cu^{2+} substitution will increase the amount of Mn^{4+} ions and decrease the amount of Mn^{3+} ions. The substitution is straight - forward for Cu^{3+} ; it only replaces Mn^{3+} ions. As a combined effect of Cu^{2+} and Cu^{3+} substitutions, the ratio of JT ions (Mn^{3+} and Cu^{2+}) to non-JT ions (Mn^{4+} and Cu^{3+}) will decrease. To further explain the correlation between GP formation and the ratio of $\text{Mn}^{3+}/\text{Mn}^{4+}$ ions, we used the model proposed by L. Downward et al., as shown in Figure 5.5. Thus, there is no observation of the appearance of GP in the $\text{La}_{0.7}\text{Sr}_{0.3}\text{Mn}_{1-x}\text{Cu}_x\text{O}_3$ ($0 \leq x \leq 0.12$) system. This is associated with the decrease in the number of JT-active ions when Cu ions exist in the sample with two valencies.

5.1.3. Determine the phase transition order and critical exponent of $\text{La}_{0.7}\text{Sr}_{0.3}\text{Mn}_{1-x}\text{Cu}_x\text{O}_3$ ($x = 0.02, 0.04, \text{ and } 0.06$) by the magnetic entropy change of the material

In this section, we utilized the method based on the relationship between magnetic entropy change and critical exponents suggested by Franco et al. to determine the nature of the PM - FM phase transition and the critical exponents. Based on the standard Arrott plots, plots of isotherms of M^2 versus M/H are constructed. The positive slopes of the Arrott plots for three samples indicate a second-order transition. However, all lines are not parallel to each other but exhibit a concave downward trend, which implies that our samples do not follow the mean-field model.

Based on the $M(H)$ data at different temperatures, the temperature dependence of magnetic entropy change $\Delta S_M(T)$ can be estimated. The plots of ΔS_M^{max} versus H data are given for three compounds fitting Equation (2.60) to the experimental data, was estimated.

Using the corresponding sets of n and δ metrics of three samples, combining two Equations (2.60) (Widom scaling equation) and Equation (2.61) (Franco et al. proposed), critical exponents β and γ are determined, including: β and γ are calculated to be 0.4372 and 1.2709 at $T = 359$ K, respectively, and 0.4641 and 1.1623 at $T = 361$ K, respectively, for the $x = 0.02$ sample; the calculated β and γ of the $x = 0.04$ sample are 0.4177 and 1.7433 at $T = 355$ K, respectively, and 0.4486 and 1.2024 at $T = 357$ K, respectively. For the $x = 0.06$ sample, β and γ are calculated to be 0.463 and 1.105 at $T = 355$ K, respectively; 0.459 and 1.013 at $T = 357$ K, respectively. The obtained critical exponents not only agree with those deduced from the KF method, but they also obey the scaling theory. These results indicate the reliability of the values estimated using the KF method.

The estimated critical exponents are close to the theoretical value obtained by the mean-field model. This result implies that long-range interactions dominate the critical behavior of the system. The substitution of Cu for Mn dilutes the magnetic lattice; however, the estimated critical parameters still have a rather small deviation from the mean field model, which may be due to the magnetic heterogeneity of the sample arising from causes such as phase separation, the effect of substitution at the B site causing magnetic dislocation from competing DE and SE interactions, or divergence of the length correlation between ferromagnetic clusters at the critical point of cation vacancy oscillations.

5.1.4. Prediction and estimation of characteristic parameters of magnetocaloric effects of $\text{La}_{0.7}\text{Sr}_{0.3}\text{Mn}_{0.92}\text{Cu}_{0.08}\text{O}_3$ and $\text{La}_{0.7}\text{Sr}_{0.3}\text{Mn}_{0.88}\text{Cu}_{0.12}\text{O}_3$ using a phenomenological model

In Section 5.1.2, the effect of Cu concentration on the ΔS_M of $\text{La}_{0.7}\text{Sr}_{0.3}\text{Mn}_{1-x}\text{Cu}_x\text{O}_3$ (system with $x = 0.02, 0.04, \text{ and } 0.06$) samples has been studied. The second-order phase transition is confirmed by the merging of rescaled ΔS_M^{max} versus T curves under the various fields. In addition, the results of temperature-dependent magnetization show that the Curie temperature decreases from 360 K ($x = 0.02$) to 357 K, and the value of ΔS_M^{max} at T_C in 10 kOe magnetic field also decreases accordingly from 1.40 J/kg.K to 1.06 J/kg.K with increasing Cu content.

Due to measurement limitations, in this section, we predicted the magnetocaloric effects in the samples $x = 0.08$ and $x = 0.12$ using a phenomenological model. Based on these results, we build a picture of the magnetic entropy change of the whole system.

In order to recognize the Cu cation substitution effect on the MCE properties in this system, the variation of ΔS_M^{max} as a function of Cu concentration (x) under an applied magnetic field of 1 T is illustrated in Fig. 5.17. It clearly shows that Cu concentration (x) increases from 0.02 to 0.04, and ΔS_M^{max} increases from 1.40 J/kgK to a maximum value of 1.47 J/kgK. A further increase in Cu concentration to the value of $x =$

0.06, the ΔS_M^{max} decreases to 1.29 J/kgK, then it increases again to ΔS_M^{max} 1.32 J/kgK when the Cu concentration is $x = 0.08$. Finally, ΔS_M^{max} reaches the value of 1.02 J/kgK for the case of a Cu concentration of $x = 0.12$. This nonmonotonic variation of ΔS_M^{max} to the Cu concentration might be explained by the fact that the oxidation state of copper in these samples can be 2+ and 3+ at samples with high Cu concentrations, which have been reported in several experimental studies.

The Curie temperature decreases to near room temperature and is decreasing but also quite high with increasing Cu concentration; therefore, these compounds become potential candidate materials for near-room temperature magnetic refrigeration applications.

5.2. Magnetic properties of the $\text{La}_{0.7}\text{Sr}_{0.3}\text{Mn}_{1-x}\text{Co}_x\text{O}_3$ ($0 \leq x \leq 1$) system

So far, there have been many studies on the magnetic properties and conductivity properties of the $\text{La}_{0.7}\text{Sr}_{0.3}\text{Mn}_{1-x}\text{Co}_x\text{O}_3$ ($0 \leq x \leq 1$) system in the world. At the Institute of Materials Science, the Vietnam Academy of Science and Technology has two theses related to this material system. Those are the theses of Assoc. Prof. Dr. Le Viet Bau (2006) and the thesis of Dr. Dinh Chi Linh (in 2021). The research content of the above two authors focuses on the magnetic lattice dilution effect, the spin glass state, the magnetocaloric effect, and the para-phase transition parameters. Up to now, the spin state of Co and the appearance of GP in the cobaltite system $\text{La}_{1-x}\text{Sr}_x\text{CoO}_3$ have been extensively studied in many works, but this issue has not been studied in the $\text{La}_{0.7}\text{Sr}_{0.3}\text{Mn}_{1-x}\text{Co}_x\text{O}_3$ system.

Therefore, in this content, we present in detail the results of the study of the spin states of Co ions, the appearance of the Griffith phase (if any), as well as the role of the Griffith phase on the physical properties of the $\text{La}_{0.7}\text{Sr}_{0.3}\text{Mn}_{1-x}\text{Co}_x\text{O}_3$ ($0 \leq x \leq 1$) system.

Polycrystalline $\text{La}_{0.7}\text{Sr}_{0.3}\text{Mn}_{1-x}\text{Co}_x\text{O}_3$ ($0, 0 \leq x \leq 1, 0$) samples were synthesized using the standard solid-state reaction method as described elsewhere. All samples did not exhibit any impurity phase, and they belonged to a rhombohedral perovskite structure with an $R\bar{3}c$ space group.

5.2.1. Spin state of the Co ion in the $\text{La}_{0.7}\text{Sr}_{0.3}\text{Mn}_{1-x}\text{Co}_x\text{O}_3$ ($0 \leq x \leq 1$) system

Fig. 5.20 shows the temperature dependence of magnetization $M(T)$ for $\text{La}_{0.7}\text{Sr}_{0.3}\text{Mn}_{1-x}\text{Co}_x\text{O}_3$ ($x = 0.0, 0.5, 0.7, 0.75, 0.8, 0.85, 0.9, \text{ and } 0.95$) under a magnetic field of 100 Oe in a field-cooled (FC) sequence. The T_C of all samples was determined by the reflection in the $dM(T)/dT$ curve. The variation in T_C with the Co doping concentration was found to be very interesting. The obtained values of $T_C = 365$ and 220 K for the $x = 0$ and $x = 1$ samples. T_C first decreased from 365 K to 80 K with the increase in

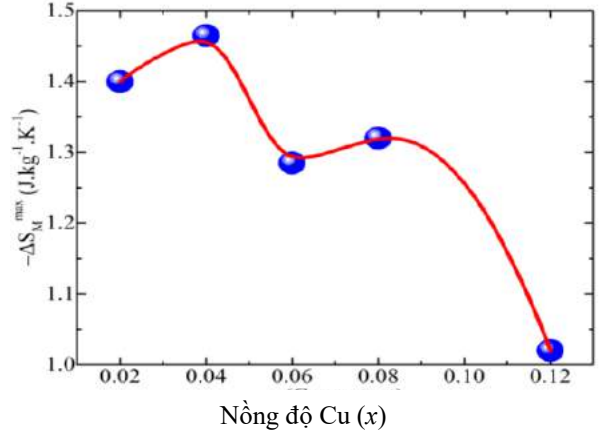


Fig. 5.17. Peak magnetic entropy of $\text{La}_{0.7}\text{Sr}_{0.3}\text{Mn}_{1-x}\text{Cu}_x\text{O}_3$ versus Cu content.

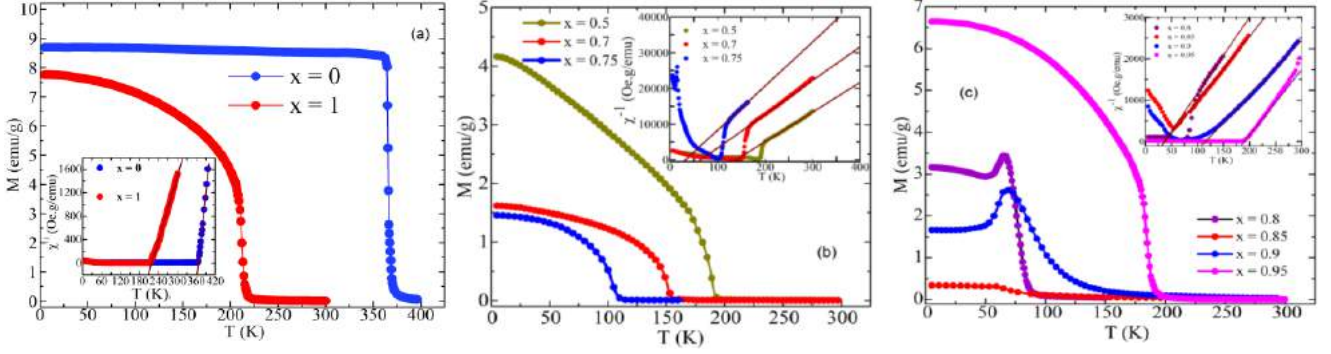


Fig. 5.20. Temperature dependence of field-cool (FC) magnetization at 100 Oe for $\text{La}_{0.7}\text{Sr}_{0.3}\text{Mn}_{1-x}\text{Co}_x\text{O}_3$ samples. The insets (a, b, and c) show the temperature dependence of the inverse DC magnetic susceptibility of $\text{La}_{0.7}\text{Sr}_{0.3}\text{Mn}_{1-x}\text{Co}_x\text{O}_3$ at 100 Oe.

cobalt concentration up to 80% ($x = 0.8$), indicating the softening of FM interactions. As the cobalt doping level further increased, T_C increased gradually from 80 K ($x = 0.8$) to 220 K ($x = 1$), which confirmed that the FM interactions in these samples were strengthened. Thus, $x = 0.8$ is the percolation threshold value of Co dopant at the Mn site, at which the T_C of the system begins to change in the opposite direction. It is clear that the effect of Co on the T_C of the for $\text{La}_{0.7}\text{Sr}_{0.3}\text{Mn}_{1-x}\text{Co}_x\text{O}_3$ system is very complex.

To understand more about the magnetic behavior of $\text{La}_{0.7}\text{Sr}_{0.3}\text{Mn}_{1-x}\text{Co}_x\text{O}_3$ ($0.0 \leq x \leq 1.0$), the relationship between the inverse susceptibility of FC and temperature [$\chi^{-1}(T)$] for all samples is plotted in the inset of Fig. 5.20. To determine the spin state of the Co ion, the inverse magnetic susceptibility $\chi^{-1}(T)$ was analyzed using the Curie–Weiss law $\chi^{-1}(T) = C/(T - \theta_{CW})$ in which, H is the applied magnetic field, $M(T)$ is magnetization, C is the Curie constant, and θ_{CW} is the Curie–Weiss temperature. It is clear that $\chi^{-1}(T)$ deviates downward from the linear Curie–Weiss behavior for the $0.5 \leq x \leq 0.8$ samples, demonstrating the existence of a new magnetic phase in the paramagnetic region of the sample. The estimated values of the Curie–Weiss temperature (θ_{CW}) and the Curie constant are listed in Table 5.5. It is possible to notice the change in θ_{CW} , similar to T_C .

From the different spin states of Co ions in cobaltite: (i) Co_{HS}^{4+} ($t_{2g}^3 e_g^2$, $S=5/2$) and Co_{LS}^{3+} ($t_{2g}^6 e_g^0$, $S=0$), (ii) Co_{IS}^{4+} ($t_{2g}^4 e_g^1$, $S=3/2$) and Co_{IS}^{3+} ($t_{2g}^5 e_g^1$, $S=1$), and (iii) mixed spin state (MS) tetravalent Co (Co_{MS}^{4+} : Co_{HS}^{4+} and Co_{IS}^{4+} ($t_{2g}^4 e_g^1$, $S=3/2$) in different proportions) and Co_{IS}^{3+} ($t_{2g}^5 e_g^1$, $S=1$), assuming that Mn^{3+} and Mn^{4+} ions exist in HS state (Mn^{3+} : $t_{2g}^3 e_g^1$, $S=2$ and Mn^{4+} : $t_{2g}^3 e_g^0$, $S=3/2$), and maintaining charge neutrality in the $\text{La}_{0.7}\text{Sr}_{0.3}\text{Mn}_{1-x}\text{Co}_x\text{O}_3$ ($0 \leq x \leq 1$) system, spin states of three cases can be considered: (I) Co^{3+} ions convert into Co^{2+} ions, (II) Co^{4+} ions convert into Co^{3+} ions, and (III) Co^{4+} ions convert into Co^{2+} ions. We have calculated the average spin value (S_{avg}) and Paramagnetic spin theory in the above cases, resulting in only case (iii) match.

Fig. 5.24 presents the experimental average spin value (S_{avg}), and the theoretical lines describe the

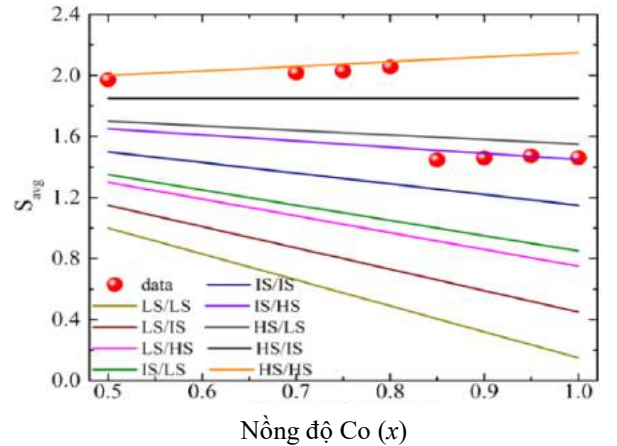


Fig. 5.24. x dependence of the average (S_{avg}) extracted from the Curie–Weiss behavior at high temperature of $\text{La}_{0.7}\text{Sr}_{0.3}\text{Mn}_{1-x}\text{Co}_x\text{O}_3$ samples. Solid lines show the behavior of the average spin value, assuming that the solid lines represent the theoretical mean spins of the different spin states of Co^{3+} and Co^{4+} ions.

different spin states of Co^{3+} and Co^{4+} ions. Clearly, the data are well fitted by the HS/HS states only for $0.5 \leq x \leq 0.8$ (orange lines), and the IS/HS states are used to describe the observed data for $0.8 < x \leq 1$ (violet lines in Fig. 5.24). Moreover, this hypothesis was consistent with the change in T_C . The competition between the FM double-exchange interaction between Mn^{4+} and Mn^{3+} and the AFM super-exchange interaction between the HS of Co^{4+} and the HS of Co^{4+} decreased T_C , which showed good agreement between the experimental results in the range of $0 < x \leq 0.8$. The presence of $\text{Co}^{3+}(\text{IS})$ and $\text{Co}^{4+}(\text{HS})$ ions in the remaining samples enhanced the FM interaction between $\text{Co}^{3+}(\text{IS})$ - $\text{Mn}^{4+}(\text{HS})$ ions, $\text{Co}^{4+}(\text{HS})$ - $\text{Mn}^{3+}(\text{HS})$, $\text{Co}^{4+}(\text{HS})$ - $\text{Mn}^{4+}(\text{HS})$ and $\text{Co}^{3+}(\text{IS})$ - $\text{Co}^{4+}(\text{HS})$ ions, so T_C increased, consistent with the experimental observations in the range of $0.8 < x \leq 1.0$.

In summary, the magnetization measurement and this hypothesis revealed that we could divide the $\text{La}_{0.7}\text{Sr}_{0.3}\text{Mn}_{1-x}\text{Co}_x\text{O}_3$ ($0 \leq x \leq 1$) compounds into two groups: (i) if the Co content is ≤ 0.8 , both the Co^{3+} and Co^{4+} ions are in the high spin state (HS/IHS), and the decrease in T_C in this region was due to the decrease in FM interactions in the compounds; and (ii) above this concentration (> 0.8), the spin states of Co ions were IS Co^{3+} and HS Co^{4+} , so T_C increased from the addition of FM interactions between HS Co^{4+} and IS Co^{3+} ions in the samples. As a result, the Co^{4+} ions are in the HS state with the increase in the Co-doping level, while the Co^{3+} ions show the spin state transition from the high spin state to the intermediate spin state at $x = 0.8$. Therefore, scenario (iii) was the most appropriate one to explain the observed magnetic properties of the studied samples.

5.2.2. The appearance of the Griffith phase in the $\text{La}_{0.7}\text{Sr}_{0.3}\text{Mn}_{1-x}\text{Co}_x\text{O}_3$ ($0 \leq x \leq 1$) system

As shown in Fig. 5.20, the inverse DC susceptibility χ^{-1} vs. T plots for all of the samples show that the samples with $0.5 \leq x \leq 0.8$ deviate downward from the linear Curie-Weiss behavior due to the positive curvature observed in the region $T_C < T < T_G$. The drastic decrease of χ^{-1} at $T_C < T < T_G$ seems to indicate the onset of a short-range FM correlation attributable to the GP response and corresponding to the existence of short-range FM spin clusters within the PM region. This can be demonstrated by ensuring that the inverse DC susceptibility $\chi^{-1}(T)$ of the four samples in the GP region reflects the following power-law behavior (1.4): $\chi^{-1} \approx (T - T_C^{\text{Rand}})^{1-\lambda_{\text{GP}}}$, $0 < \lambda < 1$.

Figure 5.26 shows $\chi^{-1}(T)$ of four samples $x = 0.5$, $x = 0.7$, $x = 0.75$, and $x = 0.8$, where the black line is the curve fitting according to Curie - Weiss law and the red line is the Griffith model fitting line. The value of the exponent λ obtained is 0.68, 0.61, 0.58, and 0.56 for samples $x = 0.5$, $x = 0.7$, $x = 0.75$, and $x = 0.8$, respectively, while T_C^{Rand} is 191

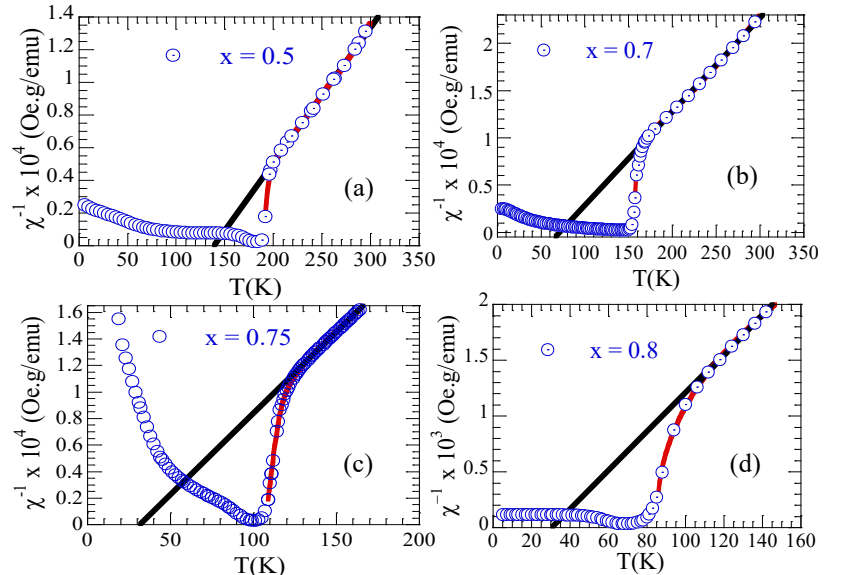


Fig. 5.26. Variation of the inverse of the susceptibility ($1/\chi$) as a function of temperature for $x = 0.5$, $x = 0.7$, $x = 0.75$ and $x = 0.8$ samples at $H = 50$ Oe. The black solid line is the best fit to the Curie-Weiss law in the paramagnetic range ($T > T_G$). The red solid lines are the fit with the power law equation $\chi^{-1}(T) \sim A(T - T_C^{\text{Rand}})^{1-\lambda}$.

K, 154 K, 112 K, and 85 K, respectively. The value of λ satisfies the condition for GP occurrence in manganites; however, it is necessary there are clearer proofs to confirm this is indeed the GP in the samples.

One of the important empirical observations confirming the existence of the Griffiths phase is the absence of spontaneity in the $T_C < T < T_G$ temperature range, i.e., the absence of a static order from long distances. Therefore, to confirm this claim, we studied the Arrott curve in the $T_C < T < T_G$ region for four samples (Figure 5.27). Our results show that this assertion is true, so the anomalous word phase on T_C in samples $x = 0.5$, $x = 0.7$, $x = 0.75$, and $x = 0.8$ is GP.

To better illustrate the above statement, we calculated the saturation magnetic moment of all three samples (theoretical and experimental) from the Arrott line at 5 K (see Figure 5.28). The results show that the experimental saturation magnetic moment decreases gradually when Co replaces Mn to the value $x = 0.8$. Then abruptly increase with $x \geq 0.85$, while the theoretical saturation magnetic moment decreases linearly in the direction of increase in the Co concentration in the sample.

The large difference between the experimental saturation magnetic moment and the theoretical saturation magnetic moment shows that the SE interaction has significantly reduced the value of μ_{sat}^{exp} .

We assume that it is the antiferrous bonds from $\text{Co}^{3+}(\text{HS})-\text{O}-\text{Co}^{4+}(\text{HS})$ that have broken the long-distance FM interactions in the sample and formed the short-distance magnetic iron clusters that are the cause of GP formation in the $0.5 < x \leq 0.8$ samples. Thus, in our samples, the appearance of GP is most likely due to the competition between AFM interactions between $\text{Mn}^{3+}-\text{O}^{2-}-\text{Mn}^{3+}$, $\text{Mn}^{4+}-\text{O}^{2-}-\text{Mn}^{4+}$ and $\text{Co}^{3+}(\text{HS})-\text{O}^{2-}-\text{Co}^{4+}(\text{HS})$ breaking the FM interaction profile of $\text{Mn}^{3+}-\text{O}^{2-}-\text{Mn}^{4+}$.

5.2.3. Phase diagram of the $\text{La}_{0.7}\text{Sr}_{0.3}\text{Mn}_{1-x}\text{Co}_x\text{O}_3$ ($0 \leq x \leq 1$) system

Figure 5.29 shows the magnetic phase diagram, which is similar to that of a single-crystal $\text{La}_{1-x}\text{Ba}_x\text{MnO}_3$ system. The phase diagram is obviously quite detailed and intricate. There are three distinct phases on the phase diagram: ferromagnetic (FM), paramagnetic (PM), and spin glass (SG) phase regions.

Based on the data of the ferromagnetic - paramagnetic phase transition, spin glass, phase transition, cloud glass, and Griffith temperature, the magnetic phase diagram of the $\text{La}_{0.7}\text{Sr}_{0.3}\text{Mn}_{1-x}\text{Co}_x\text{O}_3$ ($0 \leq x \leq 1$) system is also illustrated and presented in Figure 5.29. As shown in Figure 5.29, the phase

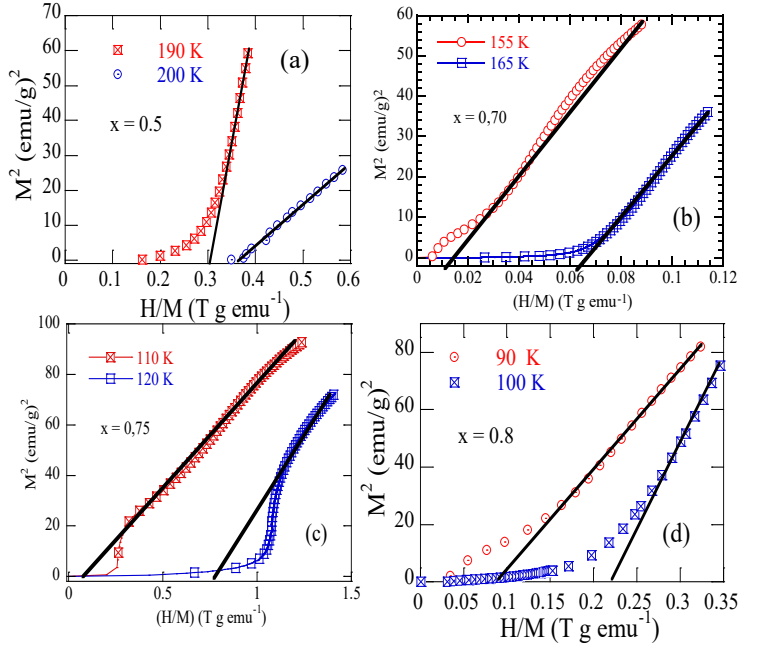


Fig. 5.27. Arrott plot M^2 vs. H/M of the isotherms collected at a temperature of $T_C < T < T_G$ for $x = 0.5$, $x = 0.7$, $x = 0.75$.

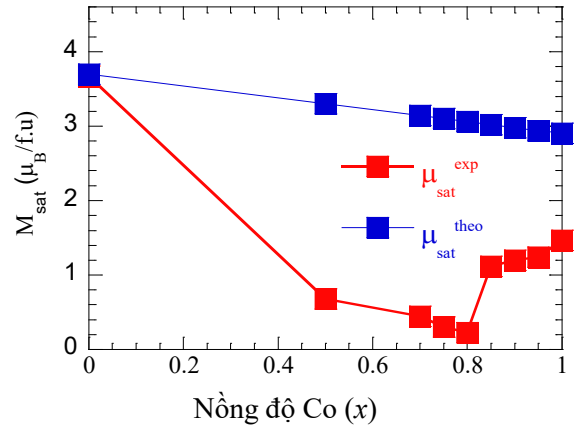


Fig 5.28. The dependence of the spontaneous magnetization on the Co concentration of $\text{La}_{0.7}\text{Sr}_{0.3}\text{Mn}_{1-x}\text{Co}_x\text{O}_3$ system.

diagram is divided into ferromagnetic (FM), paramagnetic (PM), and spin glass phase (SG) regions. In the concentration region of $0 \leq x < 0.5$, the sample shows only a single phase transition, the paramagnetic – ferromagnetic phase transition at T_C . When the concentration of Co increases in the region of $0.5 \leq x \leq 0.8$, three types of phase transitions are present: paramagnetic - GP phase transition, GP - ferromagnetic phase transition, and ferromagnetic spin glass phase transition (or spin cluster glass). Finally, in the region of $0.8 < x \leq 1$, the sample contains two types of phase transitions, which are paramagnetic - ferromagnetic and ferromagnetic - spin glass (or spin cloud glass). Because of the strong competition between the FM and AFM interactions, SG behavior in the range $0 \leq x < 0.5$ appears. Meanwhile, the GP detected in region $0.5 \leq x \leq 0.8$ is attributed to disorder-induced exchange interaction and its quenching in the present system of divalent-doped manganites.

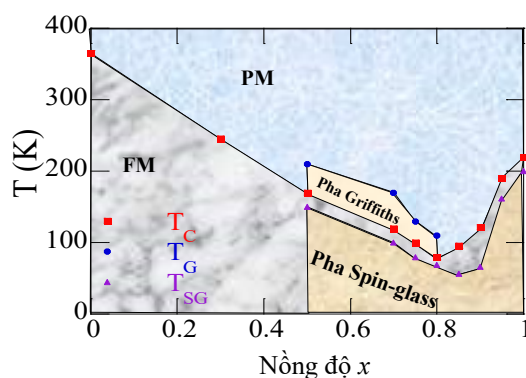


Fig. 5.29. The magnetic phase diagram of $\text{La}_{0.7}\text{Sr}_{0.3}\text{Mn}_{1-x}\text{Co}_x\text{O}_3$ ($0 \leq x \leq 1$), where FM: ferromagnetic, PM: paramagnetic.

CONCLUSIONS

From the research contents presented, some of the main results achieved by the dissertation can be summarized as follows:

1- Successfully fabricated three prototypes: (i) The nanoparticles of $\text{La}_{1-x}\text{Ca}_x\text{MnO}_3$ ($x = 0.2, 0.22,$ and 0.25) have been synthesized by the sol-gel method. The sample $\text{La}_{0.7}\text{Sr}_{0.3}\text{Mn}_{1-x}\text{Cu}_x\text{O}_3$ ($0 \leq x \leq 0.12$) system and the sample (iii) $\text{La}_{0.7}\text{Sr}_{0.3}\text{Mn}_{1-x}\text{Co}_x\text{O}_3$ ($0 \leq x \leq 1$) system by the solid-state reaction method. Except for samples $\text{La}_{0.7}\text{Sr}_{0.3}\text{Mn}_{0.92}\text{Cu}_{0.08}\text{O}_3$ and $\text{La}_{0.7}\text{Sr}_{0.3}\text{Mn}_{0.88}\text{Cu}_{0.12}\text{O}_3$ non-phase, the remaining samples are of high quality and meet the research purpose of the dissertation.

2- Study of the formation, origin, and influence of the Griffith phase (GP) on the magnetic properties of three perovskite manganites systems, including:

* The appearance of the GP in the nano $\text{La}_{1-x}\text{Ca}_x\text{MnO}_3$ ($x = 0.2, 0.22,$ and 0.25) system is related to the quenching of spin-orbit coupling. The strong antiferromagnet interaction that accompanied the quenching of spin-orbit coupling is the cause of the appearance of GP in $\text{La}_{0.78}\text{Ca}_{0.22}\text{MnO}_3$ nanoparticles. The magnetic field dependence survey of GP in two samples showed that the Griffiths coefficient decreased with the magnetic field and that the Griffiths phase was completely extinguished in the magnetic field of 10 kOe. The occurrence and suppression of the GP in both $\text{La}_{0.80}\text{Ca}_{0.20}\text{MnO}_3$ and $\text{La}_{0.75}\text{Ca}_{0.25}\text{MnO}_3$ samples are explained based on the shell-core model of the nanoscale materials.

* No observation the appearance of GP in the $\text{La}_{0.7}\text{Sr}_{0.3}\text{Mn}_{1-x}\text{Cu}_x\text{O}_3$ system ($0 \leq x \leq 0.12$). This is associated with owing to the decrease of the number of JT-active ions when Cu ions exist in the sample with two valencies +2 and +3.

* The appearance of the Griffith phase in $\text{La}_{0.7}\text{Sr}_{0.3}\text{Mn}_{1-x}\text{Co}_x\text{O}_3$ ($0.5 \leq x \leq 0.8$) is related to the competition between ferromagnetic and anti-ferromagnetic interactions of the high spin Co^{3+} and Co^{4+} ions and Mn ions in the samples.

3- Studying the effect of Griffith phase on the critical exponents, the magnetocaloric effect of the sample systems:

* The critical exponents in the samples $\text{La}_{0.75}\text{Ca}_{0.25}\text{MnO}_3$ and $\text{La}_{0.8}\text{Ca}_{0.2}\text{MnO}_3$ are close to the average field model, which is explained based on the relationship with the Griffith phase appearance. The Griffiths phase enhanced the long-range dipole–dipole interactions between the spins in the system. The critical parameters of the $\text{La}_{0.7}\text{Sr}_{0.3}\text{Mn}_{1-x}\text{Cu}_x\text{O}_3$ ($x = 0.02, 0.04, \text{ and } 0.06$) system are found from the magnetic entropy change of the sample. Then tested by the KF method and scaling theory. The results show that all three samples follow the mean field model, and both methods give the same values of the critical exponents. This adds a new method to determine the critical exponents to the MAP and KF methods.

* The magnetocaloric effect of the nano $\text{La}_{0.78}\text{Ca}_{0.22}\text{MnO}_3$ sample and the $\text{La}_{0.7}\text{Sr}_{0.3}\text{Mn}_{1-x}\text{Cu}_x\text{O}_3$ ($x = 0.08$ and 0.12) system were evaluated through $M(T)$ data at other magnetic fields using a phenomenological model. This is a simple method that predicts many physical parameters of magnetocaloric effects. The maximum magnetic entropy change in the 12 kOe magnetic field is 0,95 J/kg.K, showing that the $\text{La}_{0.78}\text{Ca}_{0.22}\text{MnO}_3$ nanomaterial holds promise for application in magnetic cooling. The presence of the Griffith phase enhanced the thermomagnetic effect in the sample. Meanwhile, the maximum magnetic entropy change according to the concentration of Cu in the system $\text{La}_{0.7}\text{Sr}_{0.3}\text{Mn}_{1-x}\text{Cu}_x\text{O}_3$ was investigated in detail according to the concentration of Cu.

4 - Based on the experimental results, a GP diagram of the $\text{La}_{1-x}\text{Ca}_x\text{MnO}_3$ ($x = 0.2, 0.22, \text{ and } 0.25$) system and a GP diagram of the $\text{La}_{0.7}\text{Sr}_{0.3}\text{Mn}_{1-x}\text{Co}_x\text{O}_3$ ($0 \leq x \leq 1$) system were constructed. The results show that the Griffith phase exists in the sample $\text{La}_{0.8}\text{Ca}_{0.2}\text{MnO}_3$, which is not observed in the bulk sample of the same composition. With the $\text{La}_{0.7}\text{Sr}_{0.3}\text{Mn}_{1-x}\text{Co}_x\text{O}_3$ ($0 \leq x \leq 1$) system, the GP phase appears in the concentration range of $0.5 \leq x \leq 0.8$ corresponding to the presence of Co^{3+} and Co^{4+} ions in the high spin state.

NEW CONTRIBUTIONS OF THE DISSERTATION

1. Study of the formation, original and influence of the Griffith phase (GP) on the magnetic properties of three perovskite manganites systems, including:

* The appearance of the GP in nano $\text{La}_{1-x}\text{Ca}_x\text{MnO}_3$ ($x = 0.2, 0.22$ and 0.25) system is related to the quenching of spin-orbit coupling. The strong antiferromagnet interaction accompanied the quenching of spin-orbit coupling is the cause of the appearance of GP in $\text{La}_{0.78}\text{Ca}_{0.22}\text{MnO}_3$ nanoparticles, whereas the occurrence and suppression of the GP in both $\text{La}_{0.80}\text{Ca}_{0.20}\text{MnO}_3$ and $\text{La}_{0.75}\text{Ca}_{0.25}\text{MnO}_3$ samples is explained based on the shell-core model of the nanoscale materials.

* No observation the appearance of GP in $\text{La}_{0.7}\text{Sr}_{0.3}\text{Mn}_{1-x}\text{Cu}_x\text{O}_3$ system ($0 \leq x \leq 0.12$). This is associated with owing to the decrease of the number of JT-active ions when Cu ions exist in the sample with two valencies +2 and +3.

* The appearance of the Griffith phase in $\text{La}_{0.7}\text{Sr}_{0.3}\text{Mn}_{1-x}\text{Co}_x\text{O}_3$ ($0.5 \leq x \leq 0.8$) is related to the competition between ferromagnetic and anti-ferromagnetic interactions of the high spin Co^{3+} and Co^{4+} ions and Mn ions in the samples.

2. Based on the experimental results, a GP diagram of the $\text{La}_{1-x}\text{Ca}_x\text{MnO}_3$ ($x = 0.2, 0.22$ and 0.25) system and a GP diagram of the $\text{La}_{0.7}\text{Sr}_{0.3}\text{Mn}_{1-x}\text{Co}_x\text{O}_3$ ($0 \leq x \leq 1$) system were constructed.

3. Successfully explain the relationship between the appearance of GP and critical behavior, magnetocaloric properties of $\text{La}_{1-x}(\text{Ca},\text{Sr})_x\text{Mn}_{1-y}(\text{Cu},\text{Co})_y\text{O}_3$ system using appropriate physical models.

LIST OF PROJECTS PUBLISHED

1. L.T.T.Ngan, N.T.Dang, N.X.Phuc, L.V.Bau, N.V.Dang, D.H.Manh, P.H.Nam, L.H.Nguyen, P.T.Phong, “Magnetic and transport behaviors of Co substitution in $\text{La}_{0.7}\text{Sr}_{0.3}\text{MnO}_3$ perovskit”, *J. Alloys Compd.*, Vol. 911, pp. 164967, 2022.
2. L. T. T. Ngan, N. T. Dang, P. H. Nam, D. T. Khan, L. H. Nguyen, L. V. Bau, N. V. Dang, V. Q. Nguyen and P. T. Phong, “Prediction of Magnetocaloric Effects of $\text{La}_{0.7}\text{Sr}_{0.3}\text{Mn}_{1-x}\text{Cu}_x\text{O}_3$ Compounds ($x = 0.08$ and 0.12) Using a Phenomenological Model”, *J. Electron. Mater.*, vol. 50, no. 3, pp. 978–986, 2021.
3. L. T. T. Ngan, P. H. Nam, N. V. Dang, L. H. Nguyen, and P. T. Phong, “Griffith-Like Phase in Co-Substituted $\text{La}_{0.7}\text{Sr}_{0.3}\text{MnO}_3$ ”, *Metall. Mater. Trans. A Phys. Metall. Mater. Sci.*, vol. 50, no. 8, pp. 3466–3471, 2019.
4. P.T. Phong, L.T.T. Ngan, L.V. Bau, N.M. An, L.T.H. Phong, N.V. Dang, and IN-JA LEE., “Critical Phenomena and Estimation of Spontaneous Magnetization by Magnetic Entropy Analysis of $\text{La}_{0.7}\text{Sr}_{0.3}\text{Mn}_{0.94}\text{Cu}_{0.06}\text{O}_3$,” *Metall. Mater. Trans. A Phys. Metall. Mater. Sci.*, vol. 49, no. 1, pp. 385–394, 2018.
5. P. T. Phong, L.T.T. Ngan, N.V. Dang, L.H. Nguyen, P.H. Nam, D.M. Thuy, N.D. Tuan, L.V. Bau, I.J. Lee., “Griffiths-like phase, critical behavior near the paramagnetic-ferromagnetic phase transition and magnetic entropy change of nanocrystalline $\text{La}_{0.75}\text{Ca}_{0.25}\text{MnO}_3$,” *J. Magn. Magn. Mater.*, vol. 449, pp. 558–566, 2018.
6. P. T. Phong, L.T.T. Ngan, L.V. Bau, P.H. Nam, P.H. Linh, N.V. Dang, In Ja Lee., “Study of critical behavior using the field dependence of magnetic entropy change in $\text{La}_{0.7}\text{Sr}_{0.3}\text{Mn}_{1-x}\text{Cu}_x\text{O}_3$ ($x = 0.02$ and 0.04),” *Ceram. Int.*, vol. 43, no. 18, pp. 16859–16865, 2017.
7. P. T. Phong, L.T.T. Ngan, L.V. Bau, N.X. Phuc, P.H. Nam, L.T.H. Phong, N.V. Dang, In-Ja Lee., “Magnetic field dependence of Griffith phase and critical behavior in $\text{La}_{0.8}\text{Ca}_{0.2}\text{MnO}_3$ nanoparticles,” *J. Magn. Magn. Mater.*, vol. 475, no. November 2018, pp. 374–381, 2019.
8. Phạm Thanh Phong, Phạm Hồng Nam, Tạ Ngọc Bách, Lưu Hữu Nguyên, Lê Viết Bá, Lê Thị Tuyết Ngân, Nguyễn Văn Đăng, “Pha Griffith và ước lượng hiệu ứng từ nhiệt trong vật liệu nano $\text{La}_{0.78}\text{Ca}_{0.22}\text{MnO}_3$,” *T. N. U. Journal*, vol. 203, no. 10, pp. 3–10, 2019.